

POLITECNICO DI TORINO

Department of Control and Computer Engineering
Master Degree in Mechatronic Engineering



Development of a Linear Axis System to Extend the Reach of Surgical Robot Arms

Supervisor:
Prof. Marco Knafitz

Candidate:
Hassan Hussein

April 2019

Declaration of Authorship

I, HASSAN HUSSEIN, declare that this thesis titled, ‘Development of a Linear Axis System to Extend the Reach of Surgical Robot Arms’ and the work presented in it are my own. I confirm that:

- This work was done wholly or mainly while in candidature for a research degree at this University.
- Where any part of this thesis has previously been submitted for a degree or any other qualification at this University or any other institution, this has been clearly stated.
- Where I have consulted the published work of others, this is always clearly attributed.
- Where I have quoted from the work of others, the source is always given. With the exception of such quotations, this thesis is entirely my own work.
- I have acknowledged all main sources of help.
- Where the thesis is based on work done by myself jointly with others, I have made clear exactly what was done by others and what I have contributed myself.

Signed:



Date:

12-04-2019

“Doing nothing is very hard to do...you never know when you’re finished.”

Leslie Nielsen

Abstract

The project was fulfilled as part of the **Minimally Invasive Robot-Assisted Computer-guided Laserosteotomy (MIRACLE)** project at the **Department of Biomedical Engineering (DBE)** at the University of Basel. Briefly, the aim of the project is to perform minimally invasive bone cutting with the assistance of robotic-guided system. For this reason a collaborative surgical robot GG-1 was designed to hold a flexible endoscope and guide it into the target zone to perform laser osteotomy. To extend the workspace of the robotic system in the operating room and increase autonomy, a new concept was introduced in the development of GG-1 platform. A linear axis system using linear servo motor technology was implemented to the robotic system. The first prototype of linear axis was developed and built in 3D printed parts with a magnetic encoder system. Due to the poor mechanical structure, the system was operating with a limited low/high speeds and lacking positioning accuracy in addition to the calibration needed at start-up.

In this thesis a new reliable linear axis system was designed and developed. Based on the defects detected in the old system and issues we had in the positioning system, the components of the previously existing prototype were revised and a literature review of different mechanisms was conducted. Several measurements were performed for the characterization of the new developed system after the successful commissioning and controller tuning. The new linear axis system showed better positioning accuracy and a smooth motion. In addition, different test movements were performed to determine the system performance. The minimum velocity the system can reach and still responds smoothly was determined. A demonstration trajectory was created showing the ability of the linear axis system in responding to different motion paths. Also, the system was tested with a load of 25 kg to verify its capability in loaded case. Although, all the tests were performed with a limited velocity. The results showed an improvement in mechanical structure and functionality.

The last task of the thesis was the implementation of admittance control concept to the linear axis system. The concept was evaluated and showed a good behaviour with the simple control algorithm used.

However, the controller parameters of the linear axis were tuned to operate with no additional load to the linear axis system. Further fine-tuning might be necessary for the full functionality of the complete robot mounted to the linear axis due to the variation in weight and inertia.

Acknowledgements

In the first place, I would like to thank my supervisor Dr. Nicolas Gerig for his great support and guidance from the beginning. This work would not have been accomplished without his outstanding assistance and time spent to clarify and discuss the work challenges to successfully complete the project. Many thanks also for Murali Karnaman for his support and follow-up during my work. Then, I would also like to thank Prof. Dr. Georg Rauter, head of the BIROMED-Lab and Professor at the Biomedical Engineering Department at the University of Basel, for giving me the opportunity to conduct my master thesis at his astonishing project. Additionally, thanks for my Prof. Dr. Marco Knäflitz from the Polytechnic University of Turin, for allowing me to conduct my thesis at the BIROMED-Lab.

Many thanks for all the BIROMED-Lab members and the entire MIRACLE team. It has been a pleasure for me working with you in a such lovely atmosphere. I enjoyed the time I spent working at the BIROMED-Lab, and I wish everyone the best with his project.

Contents

Declaration of Authorship	i
Abstract	iii
Acknowledgements	iv
List of Figures	vii
List of Tables	x
Abbreviations	xi
Symbols	xii
1 Introduction	1
1.1 Definitions	1
1.1.1 Minimally Invasive Surgery	1
1.1.2 Robotic-Assisted Surgery	2
1.2 Project MIRACLE	3
1.3 Thesis Motivation and Goals	6
2 Background	8
2.1 Robot Design Principle	8
2.1.1 Serial Robots	9
2.1.2 Parallel Robots	10
2.1.3 Hybrid Robots	13
2.2 Background on Surgical Robotic Systems	14
2.2.1 PUMA 560	15
2.2.2 PROBOT	15
2.2.3 ROBODOC	16
2.2.4 AESOP	17
2.2.5 Da Vinci	17
2.2.6 ZEUS	19
2.3 Surgical Robotic Systems Related Projects	20
2.4 GG-1 Robot	24

2.4.1	Current State	24
2.4.2	Robot Arm Features	25
2.4.3	Robot Arm Mounting in Operating Room	26
2.5	GG-1 Linear Axis System	28
3	Materials and Methods	31
3.1	Linear Axis System Main Components	31
3.2	Current State Analysis	33
3.3	Definition of Requirements	34
3.4	Solution Approach and Decision	41
3.4.1	Decision	42
3.5	Redesign	42
3.6	System Setup and Commissioning	44
3.7	Controller Tuning	48
3.7.1	Controller Overview	49
3.7.2	Low level Controller	50
3.7.3	High Level Controller	52
3.8	System Characterization	54
3.8.1	Bode Plot	55
3.8.2	Step Response	56
3.9	Test Movements	57
3.9.1	Minimum Velocity	57
3.9.2	Demonstration Trajectory	57
3.9.3	Centered Weight	58
3.10	Admittance Control Setup	59
3.10.1	Evaluation Test	60
4	Results and Discussion	62
4.1	Bode Plot	62
4.2	Step Response	64
4.3	Test Movements	66
4.3.1	Minimum Velocity	66
4.3.2	Demonstration Trajectory	67
4.3.3	Centered Weight	68
4.4	Admittance Control	69
5	Conclusion	71
A	Data sheets	73
	Bibliography	78

List of Figures

1.1	Tiny incisions done in the patient body to perform in Minimally Invasive Surgery [2].	2
1.2	Da Vinci’s surgical robotic system assisting in surgery [4].	2
1.3	Robotic setup of MIRACLE in UKA surgery [6].	3
1.4	MAKO’s surgical robotic system assisting in surgery [8][9].	4
1.5	CARLO from Advanced Osteotomy Tools [12].	4
1.6	GG-1 robotic platform.	5
1.7	First prototype of the linear axis system for GG-1	6
2.1	Serial and parallel robot structures [13].	9
2.2	Relation between forward and inverse kinematics [15].	9
2.3	Schematic of a serial robot [16].	10
2.4	Parallel robot structure [19].	11
2.5	Schematic of the Delta robot [23].	11
2.6	Demaurex’s Line-Placer installation for the packaging of pretzels in an industrial bakery [26].	12
2.7	SurgiScope in action at the Surgical Robotics Lab, Humboldt-University at Berlin [26].	12
2.8	Schematic of a planner 3 DOF’s hybrid robot structure.	14
2.9	Yamabot 10 design [29].	14
2.10	The Robotic ENT Microsurgical System (REMS) [30].	15
2.11	PUMA 560 [34].	15
2.12	PROBOT [37].	16
2.13	ROBODOC surgical robotic system [39].	16
2.14	Computer Motion’s AESOP [41].	17
2.15	Intuitive’s Surgical da Vinci [44].	18
2.16	Da Vinci’s S version with additional fourth arm [46].	19
2.17	Da Vinci’s SP version and the single multi-wristed arm [51].	19
2.18	ZEUS Robotic Surgical System’s console (A) and slave arms (B) [53].	20
2.19	CARLO from Advanced Osteotomy Tools [12].	21
2.20	MAKO surgical robotic system [8].	21
2.21	Latest version of Galen surgical robot [56].	22
2.22	DLR Miro surgical robot arm [58].	22
2.23	Versius surgical robotic system [60].	22
2.24	I-SUR robotic platform [62].	23
2.25	GG-1 platform CAD design.	24

2.26	From left to the right: KUKA Ibr Med 7 R 800 from KUKA (Germany), UR3 from Universal Robots (Denmark) and DLR MIRO from DLR (Germany) [63][64][58].	26
2.27	CAD design of GG-1 first prototype robotic platform.	27
2.28	DLR Miro surgical robotic arms [66].	27
2.29	KUKA's Linear Unit [65].	28
2.30	GG-1 collaborative feature.	29
2.31	Surgical robotic system covered during surgery[69].	30
3.1	Linear axis systems existing mechanisms, Ball-Screw, Rack & Pinion and the Belt-Drive [70][71][72].	31
3.2	Linear axis system first prototype main components.	32
3.3	Linear servomotor main parts [73].	33
3.4	Linear servomotor working principle[74].	33
3.5	Carriage bending due to magnetic attraction force.	34
3.6	Magnetic attraction force generated between the coil unit and the permanent magnets [75].	34
3.7	The direct contact between the coil unit and the permanent magnets and lack of the required air gap.	35
3.8	Misalignment of bearings screws.	35
3.9	Stacking zone of the coil part and magnets.	35
3.10	Magnetic Encoder System (MES) by Beckhoff Automation.	35
3.11	Ball and lead screw drive mechanisms [77].	36
3.12	Belt drive (left) and Rack & Pinion (right) drive mechanisms [79][71].	37
3.13	Round linear guide[82].	38
3.14	Square linear guide [84].	39
3.15	Optical encoder working principle [86].	40
3.16	LC 115 absolute linear encoder system from HEIDENHAIN [88].	41
3.17	CAD design of the carriage.	43
3.18	Figure showing the required air gap between the coil and unit.	43
3.19	Slide stops CAD design.	43
3.20	Robot arm mounting parts designed in SolidWorks.	44
3.21	CAD design of full linear axis system.	44
3.22	CAD design of the full robotic system.	45
3.23	Optional encoder card from Beckhoff [89].	45
3.24	Single permanent magnet plate.	46
3.25	The new developed linear axis system full assembly.	46
3.26	TwinCAT drive manager.	47
3.27	P-0-0166 command window in TwinCAT drive manager.	48
3.28	P-0-0166 command window in TwinCAT drive manager after execution.	48
3.29	System closed-loop control representation.	49
3.30	Parallel configuration of the PID controller [90].	49
3.31	System controller overview.	50
3.32	TwinCAT Control Drive Manager (TCDM) showing the three blocks of the controller.	51
3.33	Velocity Input command.	53
3.34	Velocity controller new parameters in TCDM.	53

3.35	Simulink model of the high level controller.	53
3.36	Graphical representation of high level parameters tuning.	54
3.37	System state in tuning the controller parameters.	55
3.38	An example of a system step response demonstrating the main parameters of the step response to analyze.	56
3.39	Demonstration trajectory consisting of four parts created for testing our system.	57
3.40	Centered weight of 25 Kg for testing system performance.	59
3.41	Admittance control setup.	59
3.42	First part of the simulink model for admittance control.	60
3.43	Second part of the simulink model for admittance control.	60
3.44	Admittance control evaluation test.	61
4.1	Magnitude plot.	63
4.2	Phase Plot.	63
4.3	Rise time results.	64
4.4	Overshoot results.	65
4.5	Settling time results	65
4.6	Steady state error.	66
4.7	Minimum velocity test performed, starting with a velocity of 1 mm/s to reach a minimum of 25 μ m.	67
4.8	Figure showing both desired and measured trajectories.	67
4.9	Centered weight of 25 Kg added to the system for testing performance.	69
4.10	Admittance control evaluation test.	70
A.1	LC 115 data sheet from HEIDENHAIN manual	74
A.2	Manual linear servomotor AL2412 from Beckhoff	76
A.3	Magnetic Encoder System (MES) properties from Beckhoff	77
A.4	Linear guide rails and ball bearing carriages properties from ITEM.	77

List of Tables

2.1	Characteristics of serial and parallel robots.	13
2.2	Surgical robot arms features.	26
3.1	Table comparing the different drive train mechanisms for the linear axis system [81].	38
3.2	Table of Ziegler-Nichols method showing the PI and PD type controllers [91].	51
3.3	Table showing the tuned parameters of the new linear axis system overall controller.	54
3.4	Frequency values used for Bode Plot.	55
3.5	Step sizes chosen for plotting the step response.	56
4.1	Bode plot recorded data, ω is the frequency used for our plot, A_{out} is the output amplitude of the sine signals in meters, δt is the time shift between the Input and output signals in ms, and T is the oscillation period of the output signal in ms.	62
4.2	Results of the step response test done at different step sizes.	64

Abbreviations

MIS	Minimally Invasive Surgery
MIRACLE	Minimally Invasive Robot-Assisted Computer-guided LaserosteotomE
UKA	Unicompartmental Knee Arthroplasty
OR	Operating Room
3D	Three Dimensional
CAD	Computer Aided Design
DoF	Degree of Freedom
CNC	Computer Numerical Control

Symbols

ω	angular frequency	rads^{-1}
A	amplitude	m
T	Period	sec

Chapter 1

Introduction

The thesis is divided into five chapters, the first chapter gives an overview of the project in which the master thesis was conducted, highlighting the current state of the project and thesis motivation and goals. The second chapter provides a background on robotic structure design and existing robotic surgical systems. Additionally, the surgical robotic system (GG-1) developed at DBE and its exclusive feature, the linear axis system. The third chapter describes the methods used including analysis and redesign, controller tuning, characterization, test movements and implementation of admittance control for the new linear axis system. In the fourth chapter results of performed tests and system characterization are reported and discussed. Lastly, chapter five concludes the entire thesis work.

1.1 Definitions

Primarily, a brief description of two main terms used in the thesis are defined, *Minimally Invasive Surgery* and *Robotic-Assisted Surgery*.

1.1.1 Minimally Invasive Surgery

Compared to the conventional open surgery, Minimally Invasive Surgery (MIS) is an alternative method for performing the procedures. Through small incisions made in the patient body targeting a specific location, miniature surgical tools (Fig. 1.1) are inserted including a tiny camera to perform the surgery [1].



FIGURE 1.1: Tiny incisions done in the patient body to perform in Minimally Invasive Surgery [2].

1.1.2 Robotic-Assisted Surgery

Robotic-assisted surgery is also a type of minimally invasive procedure that uses small incisions. The difference is instead of the surgeon using their hands to manually control the camera and tools, they use the power and high precision of robot technology (Fig. 1.2)[3].



FIGURE 1.2: Da Vinci's surgical robotic system assisting in surgery [4].

1.2 Project MIRACLE

This work was fulfilled under the umbrella of the project **MIRACLE**, a flagship project of the Department of Biomedical Engineering at the University of Basel. The project is funded by Werner Siemens-Foundation¹ and aims to develop a robotic endoscope contact-free bone surgery with laser beam (Fig. 1.3). Different groups are working together to fulfill the goal of this project, ranging from robotics and laser technology to virtual planning and customized implants. The first application for the robotic system is the Unicompartmental Knee Arthroplasty (UKA), a surgical procedure used to relieve arthritis in one of the knee compartments in which the damaged parts of the knee are replaced [5]. MIRACLE is intended to be applied later in other applications like cranio-maxillofacial surgery, neurosurgery, otolaryngology, traumatology, and spinal column surgery.

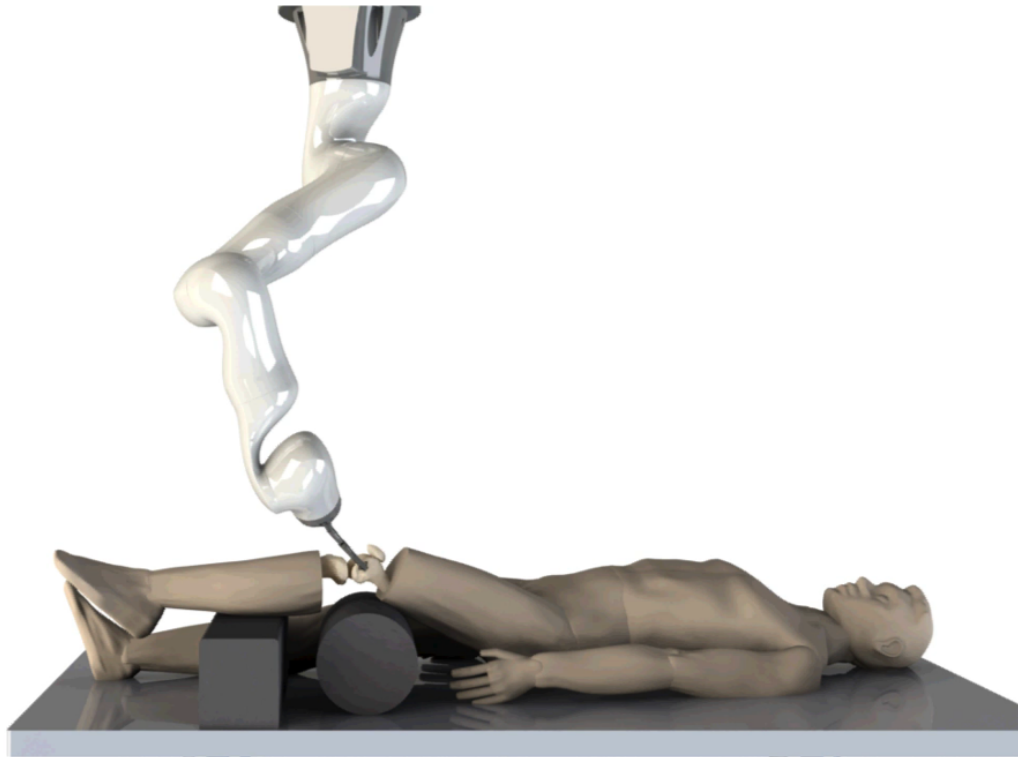


FIGURE 1.3: Robotic setup of MIRACLE in UKA surgery [6].

In an effort to reduce the side effects of the conventional UKA surgery, a robotic-assisted system MAKO² for partial-knee arthroplasties and total hip replacements was developed in 2006 for assisting in surgery. MAKO (Fig. 1.4) is robotic-arm with a tactile

¹Werner Siemens-Foundation, Zug, Switzerland

²Stryker Corporation, Kalamazoo, MI, U.S.A.

guidance system, helps the surgeon in performing the operation based on personalized pre-operative plan for the target zone [7]. Although the system offers some unique technical advantages over conventional procedure, conventional tools for cutting and drilling like saws and drills are still required to perform the surgery.

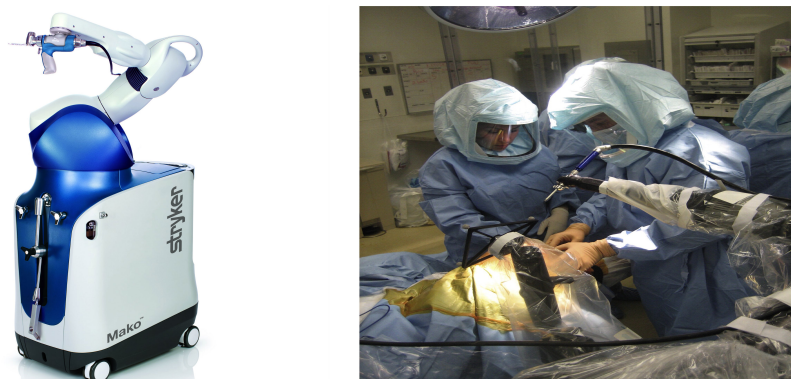


FIGURE 1.4: MAKO's surgical robotic system assisting in surgery [8][9].

Differently, an alternative robotic-assisted technology that will be implemented in orthopedic field and bone cutting is the laser osteotomy. Laser osteotomy offers precise bone cuts of different geometries compared to the conventional bone surgery, where the use of mechanical tools can cause trauma and delayed healing time. CARLO³ system (short for **C**omputer **A**ssisted **R**obot-guided **L**aser **O**steotome) was founded in 2010, in which the robot uses the laser beam to cut through bone precisely and without contact [10]. CARLO system is still undergoing clinical trials and will become the first robotic system that can cut bone without contact and with cold laser technology [11].

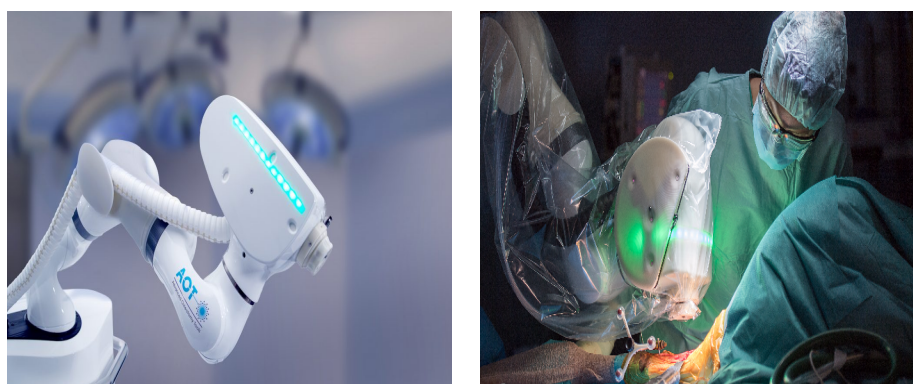


FIGURE 1.5: CARLO from Advanced Osteotomy Tools [12].

Both approaches require an open surgery, an incision of few centimeters is made in the patient body for the conventional tools or the laser beam to cut. On the contrary,

³Advanced Osteotomy Tools - AOT AG, Basel, Switzerland

MIRACLE is aiming to perform these types of surgery with the MIS approach, through a tiny incision in the skin, an endoscope is inserted and fixed to the bone and the laser beam can be positioned by actuating the end-effector (tip of endoscope).

For achieving this goal, the **Bio-Inspired RObots for MEDicine Laboratory** (BIROMED-Lab) at the DBE, develops bio-inspired robotic and mechatronic systems for medical applications. An entirely surgical platform is being developed consisting of different sub-systems like a flexible endoscope for single port surgery, a positioning and stabilization mechanism at the tip of the robotic endoscope, a robotic platform (GG-1) that allows precise control of the flexible endoscope, in addition to new technologies in force sensing for endoscopes, an intuitive telemanipulation interface, a highly integrated optics and spray system for endoscopic laser surgery.

One part of the project is the development of a collaborative robot (GG-1) capable of holding and positioning the flexoscope precisely in the targeted site. Allowing the surgeon to interact with the robot in a collaborative manner. The aim is reducing the set up time needed for the surgical procedures by providing low level autonomy to the robot while keeping the surgeon in charge of high-level decisions. Further more, details on the features and challenges of conducting the robotic platform will be discussed in section 2.4. GG-1 is controlled in real-time system to guarantee deterministic response times, by providing the angle positions of each joint, the robot is able to move to any position in the defined workspace. Due to the poor structure of the current robotic platform, limitations in terms of velocity, travel length, and joints workspace have been defined.

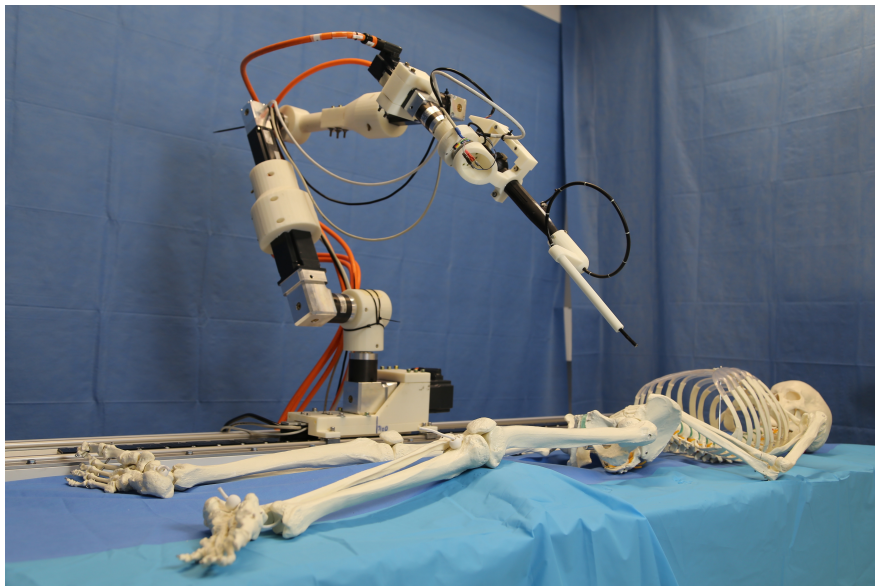


FIGURE 1.6: GG-1 robotic platform.

1.3 Thesis Motivation and Goals

Although the current robotic system is working under these limitations, the goal is to develop a reliable robotic system meeting the conventional features of a surgical robotic system. Main features like workspace, positioning accuracy, remote center of motion, tremor compensation and gravity compensation have to be considered. To realize these features we need a rigid mechanical design for our system. Redesigning the remaining robot arm will be a future project based on further requirements from the clinical partners that were still under development during the period of the current thesis. However, based on the current system we considered it reasonable for the moment to solve the issues we have in the the linear axis unit (prismatic joint) (Fig. 1.7). Being the base joint of the full robotic arm and the first Degree of freedom (DoF), having a reliable and rigid structure of this part can facilitate the redesign and control of the full arm later, offering the user the ability to move with any desired velocity confidently, under safe conditions.

The mechanical structure of the linear axis results in some defects, limiting the system to move with a velocity of 1 cm/s along the rail. Also, the feedback system used provides an absolute positioning information only if it is homed correctly. Therefore, not providing any benefit compared to a relative encoder with calibration and would not allow homing or calibration-free setup. Moreover, the last time we tried to run the system, the linear axis sledge got stuck due to the defects we have in the current system.

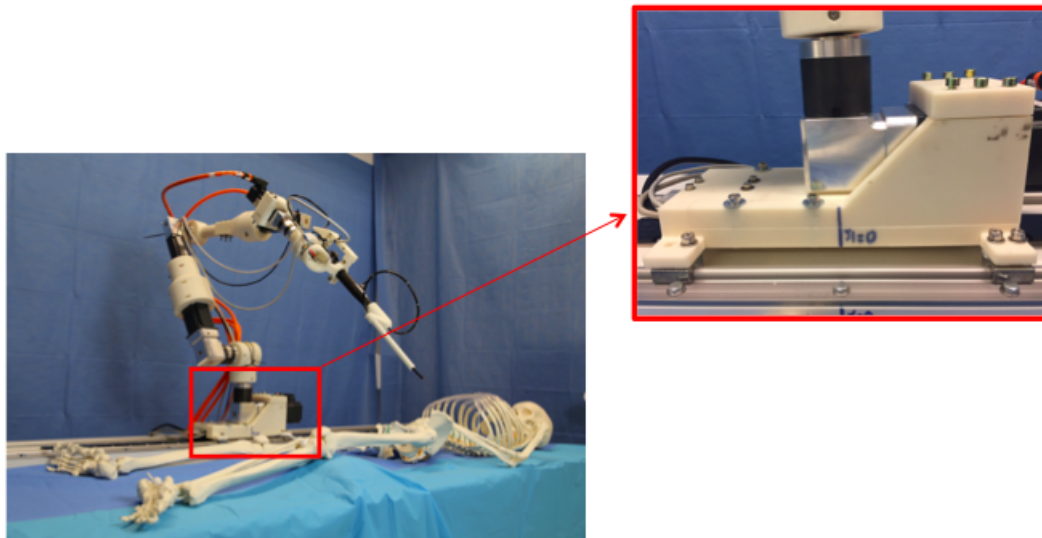


FIGURE 1.7: First prototype of the linear axis system for GG-1

Based on these issues and limitations of the current linear axis system for our GG-1, the main goal of the thesis is to develop a new reliable linear axis system able to support and guide smoothly the robot arm, with an absolute positioning sensor. Consequently,

as mentioned before, the goal of the whole project is developing a collaborative robot arm through the use of admittance control approach. One task of the thesis is the implementation of the admittance control only along the new designed linear axis system. Listed below are the steps followed to conduct the master thesis project for achieving the thesis goal.

- Literature research conducted for surgical robotic systems
- Mechanical review of the current linear axis system
- Redesign a new rigid linear axis system with a full absolute feedback system
- Implement the admittance control to the developed linear axis system

Chapter 2

Background

In this chapter, the different robot designs are illustrated and an overview on the history of surgical robotics is given, with a brief description of each. In addition to some ongoing and completed related projects in the field of surgical robotics. After that, moving to the robotic platform GG-1 developed at the DBE, introducing the main components and features of the robot and comparing it with other existing surgical robotic systems regarding the arm features and mounting options in the operating room. Lastly, ending up with the particular feature of the robotic system GG-1 and the main thesis focus, the linear axis system, highlighting its current state.

2.1 Robot Design Principle

Nowadays, robot manipulators are being used in wide variety of applications in the industry. These manipulators utilization range from simple tasks, like pick and place to more sophisticated ones like micro-chip assembly. Because industry demands manipulators that increase productivity and quality at reduced manufacturing costs, the goal of engineers is to design cost-effective manipulators with high dexterity and robust functionality. To be able to achieve these features, not only the design of advanced controller algorithms is recommended but the robot architecture must provide a high robustness and dexterity.

In designing a robot, a group of links are connected by joints forming a kinematic architecture. Based on the arrangement of these links, two main types of robot result, serial and parallel robot or manipulator as shown in figure 2.1. Each of these robots have its advantages and disadvantages. Both structures will be discussed in details in the next sections.

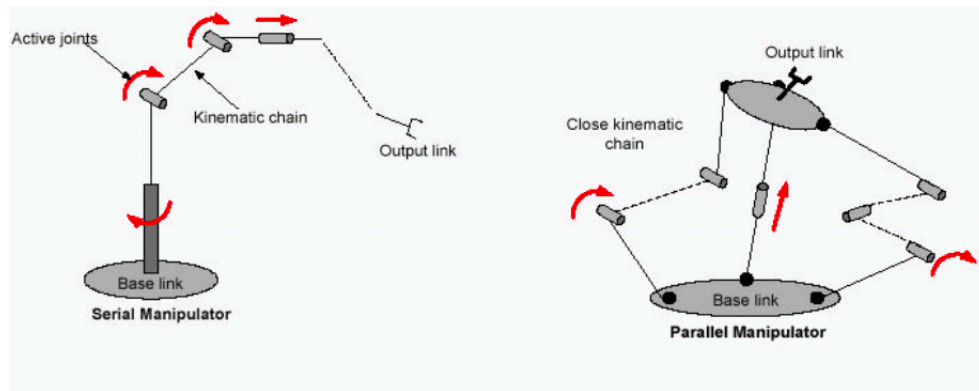


FIGURE 2.1: Serial and parallel robot structures [13].

Generally, a robot to perform a specific task, the location of the end effector relative to the base has to be defined first. This is called position analysis problem. Two main types of position analysis problems exist; The direct position or forward kinematic problem and the inverse position or inverse kinematic problem [14]. Usually, in forward kinematics, the joint variables are given and the problem is to find the location of end effector. On the contrary, for inverse kinematics, the location of the end effector is given and the problem is to find the joint variables necessary to bring end effector to a desired position.

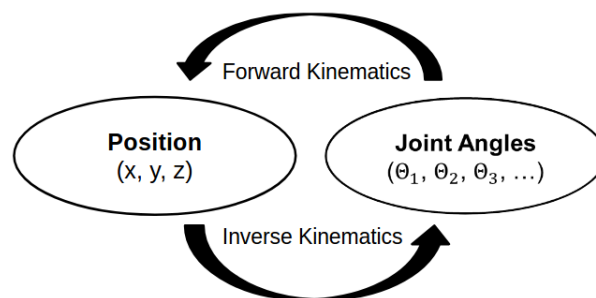


FIGURE 2.2: Relation between forward and inverse kinematics [15].

2.1.1 Serial Robots

Serial robot has its links arranged serially as the name indicates. Each link is connected by its predecessor and its successor by a one DoF joint. For example, in rotational joint, allowing the rotation of a rigid body around an axis, or in prismatic joint the translational motion along an axis. Basically, one end of the serial robot is fixed and the other is free, called the end effector (Fig. 2.3). Based on the number of joints or DoF's used, this configuration offers a wide range for the end effector to reach or the so

called workspace. A large workspace is a crucial characteristic for the industrial usage, where more tasks can be achieved using minimum number of robots. A second advantage

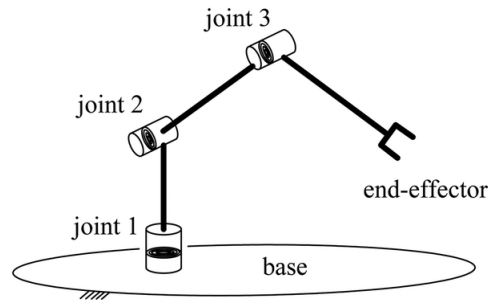


FIGURE 2.3: Schematic of a serial robot [16].

of serial robots is the simplicity of solving the forward kinematics, while solving the inverse kinematics is more challenging. Denavit-Hartenberg (DH) is a commonly used convention for attaching coordinate frames to the joints of a kinematic chain. More detailed explanation for DH approach can be found in the book '*Kinematic synthesis of linkages*' [17].

Nevertheless, serial robots offers a large work space and easy forward kinematics, positioning of the end effector lacks accuracy. Theoretically, the joint positioning errors of the serial robot are accumulated causing a position error at the end effector between the desired and the actual position. Accuracy can be affected also by additional factors like design defects, gear and joint backlash, rigidity of the robot structure, flexibility effects such as the bending of the links under gravitational and other loads and many other factors.

2.1.2 Parallel Robots

A parallel robot manipulator is composed of two or more closed-loop kinematic chains in which the end-effector is connected to the fixed base by at least two independent kinematic chains (Fig. 2.4). Between the base and the end-effector platforms are serial chains (called legs or limbs). The first use of this type of mechanism initiated in the early 1960's, when the first flight simulators were built [14]. Since then, parallel manipulators have been studied by numerous researches [18].

Due to closed kinematic chain design and the implementation of several limbs, the range of motion of the end-effector is restricted resulting in a small useful workspace. However, solving the inverse kinematics in parallel robots is fairly straightforward, the forward kinematics is more complicated. The difficulty in solving the forward kinematics is

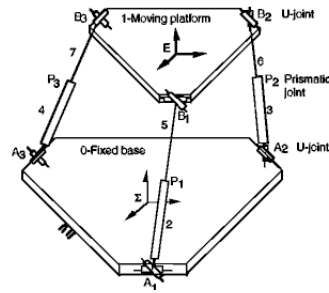


FIGURE 2.4: Parallel robot structure [19].

mainly due to existence of the multiple closed-loop chains in the parallel structure. Several approaches have been proposed for solving the forward problem, including Newton-Euler formulation, Lagrangian formulation and principle of virtual work [20][21][22].

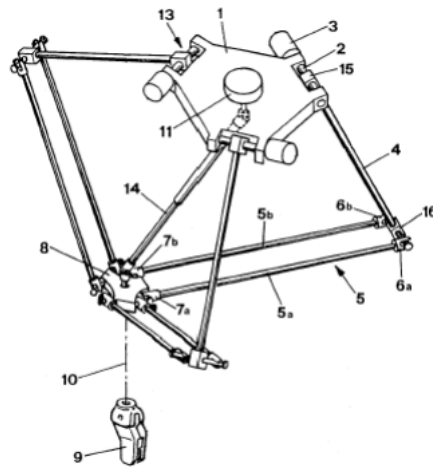


FIGURE 2.5: Schematic of the Delta robot [23].

The main feature regarding the parallel design is the accuracy and positioning, where the position errors of the links at the end-effector are averaged and not accumulated as in the serial robot. Moreover, the use of multiple chains generates a higher architectural stiffness and accuracy [24]. A study has been conducted using two serial and two parallel 2-DOF planar robots where the input errors are the only source of inaccuracy [25]. The study showed a slightly improvement in the accuracy of the parallel structure compared to the serial robot. Based on this experiment, we cannot generally state that parallel structure is in favor, because the study was done on a simple and limited case.

One example of a successful parallel kinematic robot structure is the Delta robot (Fig. 2.5) designed in the 80's by Prof. Raymond Clavel¹. The reason for this success is that the features of this structure fit into applications requiring very fast handling of light

¹Professor at École Polytechnique Fédérale de Lausanne - EPFL

weight products, for example in consumer goods, food and electronics industries. The marketing of the delta robot started long time ago where the licence was bought first by the Swiss company *Demaurex* that started commercializing it for packaging industry (Fig. 2.6). Another licence was sold to the Swedish company *Elekta*, specialized in the surgical domain and it manufactured a Delta robot used to carry a heavy (20 kg) microscope as seen in figure 2.7 [26].



FIGURE 2.6: Demaurex’s Line-Placer installation for the packaging of pretzels in an industrial bakery [26].



FIGURE 2.7: SurgiScope in action at the Surgical Robotics Lab, Humboldt-University at Berlin [26].

The Delta robot design has attracted great interest not only in the industry field but also the research labs. A number of variants have been proposed in the literature but most of those that have been prototyped remained close to the original design.

2.1.3 Hybrid Robots

After we have seen the advantages and disadvantages of both robot structures, the main features of each is illustrated in the table 2.2. Based on the table comparison, it is clear that serial structure is a preferred choice in terms of workspace and simple forward kinematics, while solving the inverse kinematics, the parallel is favored. The balance between serial and parallel structures is often inclined by the application of specific requirements that may impose one of these architectures. The selection depends on many different factors like, type of application (repetitive, precise, etc.), task requirements (DOF's, speed, accuracy, etc.) as well as, load requirements, workspace, programming time and other factors.

Feature	Serial robot	Parallel robot
Workspace	Large	Small
Forward kinematics	Easy	Difficult
Inverse Kinematics	Difficult	Easy

TABLE 2.1: Characteristics of serial and parallel robots.

A new idea of combining both structures has been established in the past, called the hybrid structure (Fig. 2.8). A hybrid structure is a combination of closed-chain and open-chain mechanisms [27]. Hybrid structures are in fact compromise between advantages and disadvantages of both robots, serial and parallel. This type overcomes the limited workspace of the parallel manipulators and the low position accuracy of the serial manipulators.

Currently, there has been an increasing interest in the hybrid robot manipulators although little literature on these manipulators is available. An example of this structure is a novel project called Yamabot 10 (Fig. 2.9). The combined architecture of a serial and delta robot gives some benefits, for instance in the investigation of workspace, in which the main workspace is provided by the serial robot, so the delta robot has its own small workspace. In the research paper [28], design , analysis and forward kinematics of hybrid manipulator are investigated and explained.

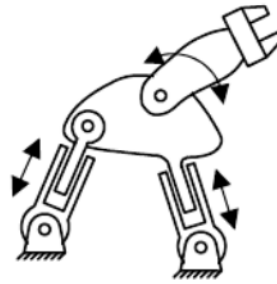


FIGURE 2.8: Schematic of a planar 3 DOF's hybrid robot structure.



FIGURE 2.9: Yamabot 10 design [29].

Although, this structure of robots is still not widely used, various projects of surgical robotic systems have already realized the idea of combining both features. For example, the Robotic ENT (Ear, Nose, and Throat) Microsurgery System (REMS) developed by Galen Robotics Inc. within the Laboratory for Computational Sensing and Robotics at Johns Hopkins University is a type of hybrid structure (Fig. 2.10) [30]. The base of REMS is a Delta stage formed of three linear actuators, the roll motion and tilt motion at the proximal and distal ends of the arm add two DoF's to the system. This type of combination is a promising field in the near future.

2.2 Background on Surgical Robotic Systems

The initial medical robots devised in the 1980's were autonomous industrial robots that had been applied to clinical problems. These included a stereotaxic needle placement system for neurosurgery and robots for orthopedic applications [31]. Neurosurgery and orthopedics were the first applications for surgical robots because they could be interfaced with image guidance systems and the rigid nature of the anatomy allowed for autonomous positioning of the surgical tools [32].

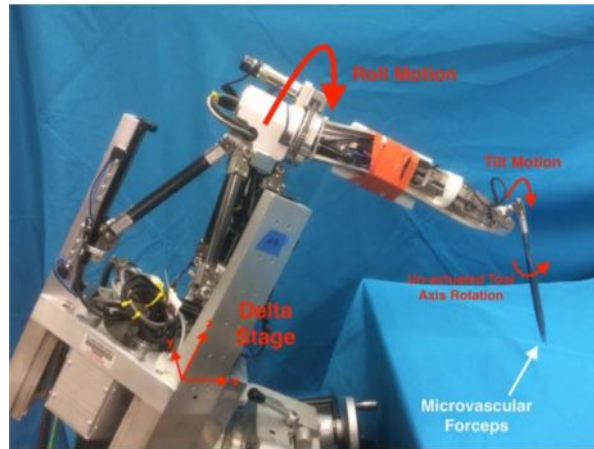


FIGURE 2.10: The Robotic ENT Microsurgical System (REMS) [30].

2.2.1 PUMA 560

The first robot-assisted surgical procedure reported in the literature was in 1985, when an industrial robotic arm (Fig. 2.11) was modified to perform a stereo-tactic brain biopsy with 0.05 mm accuracy [31][33]. The PUMA (Programmable Universal Machine for Assembly) was used for holding and manipulating a biopsy cannula, a procedure previously subject to error from hand tremors during needle placement. Based on it, several research programs were initiated.



FIGURE 2.11: PUMA 560 [34].

2.2.2 PROBOT

In 1988, "Brian Davies", a medical robotic professor at the Imperial College in London, designed a robot (with help of colleagues) that could remove soft tissue from a person (Fig. 2.12) [35]. It was one of the first robots to do so, the robot allows surgeons to specify the correct cutting sequence to remove tissue. The system was used specifically

for trans-urethral resection of prostate, a procedure that required numerous repetitive cutting motions [36].

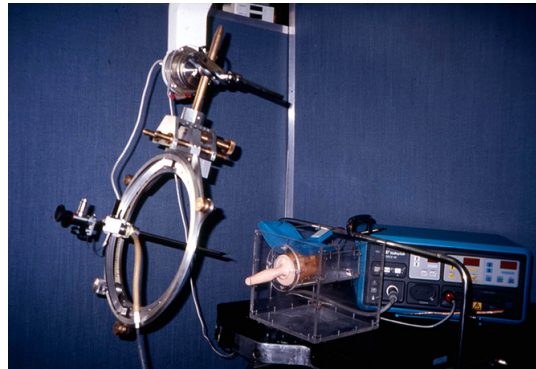


FIGURE 2.12: PROBOT [37].

2.2.3 ROBODOC

In 1992, the ROBODOC surgical robotic system was developed by the American companies Integrated Surgical Systems, Inc.(ISS) and International Business Machine Cooperation (IBM). It was mainly used for hip replacement surgery. The ROBODOC is a computer-guided mill used to core the femoral head to receive a hip replacement prosthesis. The use of ROBODOC in orthopaedic procedure demonstrated a high accuracy compared to the conventional techniques [33]. Similar devices have been designed also for use in bone surgery, notably the Acrobot² and the Staubli RX-130³ robot. Neither device has yet completed clinical testing nor received Food and Drug Administration(FDA) approval [38].



FIGURE 2.13: ROBODOC surgical robotic system [39].

²The Acrobot Company, Ltd., London, UK

³Staubli Unimation Inc., Faverges, France

2.2.4 AESOP

The first robotic system designed for abdominal procedures was developed in 1994 by Computer Motion⁴, the AESOP (Automated Endoscopic System for Optimal Positioning) (Fig. 2.14). The AESOP allowed the surgeons to control the orientation of the traditional laparoscope via foot pedal and later voice commands, freeing the hands of the surgeon for surgery. It was the first voice-controlled robot to receive FDA approval [40].



FIGURE 2.14: Computer Motion's AESOP [41].

2.2.5 Da Vinci

In 2000, a new robotic surgical system was developed by the American company Intuitive Surgical Inc., the *da Vinci* surgical system. *Da Vinci* was different of what other companies were doing in the field of robotic-assisted technology since the idea was to facilitate the complex surgeries using minimally invasive and tele-manipulation approaches. The system overcame the limitations that were put forward by the conventional laparoscopic systems [42]. Specifically, the surgeon discomfort due to the inconvenient stance and fatigue during long operations. These restrictions could be overcome by articulating and controlling the tips of instruments from a separated console and thereby, improving the range of motion and dexterity during operation [43].

The *da Vinci* System consists mainly of three components: a surgeon console with an integrated three-dimensional display stereo viewer, a robotic manipulator with mounted arms and a vision cart as seen in figure 2.15 [45]. With *da Vinci*, small incisions are made to insert the miniaturized wristed instruments and a high-definition camera. The surgeon seated at a console few feet away from the patient views an actual image of the surgical field while operating in real-time. In addition, the surgeon uses the console's

⁴Computer Motion, Santa Barbara, Ca, U.S.A.



FIGURE 2.15: Intuitive’s Surgical da Vinci [44].

master controls to maneuver the patient-side cart’s robotic arms. According to the manufacturer, the instruments exceed the natural range of motion of human hand where these robot arms follow the surgeon hand motions with motion scaling and tremor reduction to achieve more precise movements on the surgical site.

In 2006, Intuitive Surgical upgraded their system (*S* version) by inclusion of a fourth instrument arm (Fig. 2.16). In addition to the greater workspace via instrument extension and increased range of movement, the new version introduced “high-definition imaging and Pro multi-image display”. This particular feature provides the surgeon with additional information from auxiliary video signals (e.g. CT or ultrasound images). In 2009, the *Si* version was released adding a dual console that allows two surgeons to work collaboratively. This feature offers more training for surgeons unfamiliar with robotic-assisted surgery. Moreover, the *Si* enhanced the surgeon’s control and vision with simplified control foot-switch and further ergonomic settings.

The *da Vinci Xi* was released in 2014 providing improvements in architecture compared to the *Si* version in addition to new features. For example, the redesigned 8-mm endoscope, where the camera, cable and endoscope have been integrated into a small composition. Compared to the earlier version of Da Vinci which could only be inserted through 12-mm ports. Another feature is the axial rotation of the arm joints, where at maximum instrument reach the *Xi* arms gain 28° of movement over the *Si* version [47]. The fourth and latest generation of da Vinci system was the *da Vinci SP* or the single-port (Fig. 2.17). With the da Vinci SP, a single arm delivers three multi-jointed instruments and a fully wristed 3D HD camera for visibility and control in narrow and



FIGURE 2.16: Da Vinci's S version with additional fourth arm [46].

deep surgical spaces[48][49]. In May 2018, Intuitive Surgical announced the new FDA clearance for the da Vinci *SP* for urologic surgical procedures that are performed by single port approach [50].



FIGURE 2.17: Da Vinci's SP version and the single multi-wristed arm [51].

2.2.6 ZEUS

ZEUS Robotic Surgical System (ZRSS) was developed by the American company Computer Motion for assisting in surgery. It received the FDA approval in 2001 after seven years of launching its predecessor AESOP. ZRSS compose of three arms, the first arm is a AESOP, voice-activated endoscope assisting the surgeon to view clearly inside the patient's body. The other two arms mirror the surgeon movements to execute more precise incisions and extractions. The robot arms were designed to minimize the surgeon tremor

during the surgery, especially during operations that last for several hours. During the surgery the surgeon sits at the ZEUS console (Fig. 2.18) and control the robotic arms to perform the procedure. In 2003, the merge of the company Computer Motion with its rival Intuitive Surgical led to the discontinuity of the development of the ZEUS system. The merge of the two companies combined their efforts to develop an innovative robotic surgical system, the *da Vinci* [52].

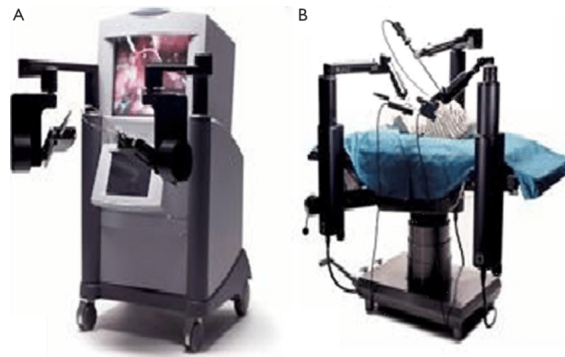


FIGURE 2.18: ZEUS Robotic Surgical System's console (A) and slave arms (B) [53].

2.3 Surgical Robotic Systems Related Projects

In addition to the above surgical robotic systems, numerous projects were initiated in the recent years for the same interest. Some of these projects are still in the development stage and trial while others started in commercializing their products. The listed projects below were intended for use in different surgical procedures and applications.

1. Cold Ablation Robot-guided Laser Osteotome (CARLO)

- CARLO is a robot-guided device for cutting bone with laser as mentioned before. Developed at Advanced Osteotomy Tools (AOT) in Switzerland. A collaborative KUKA⁵ robot arm used with customized laser head device mounted to the robot arm for performing the bone cut as seen in the figure 2.19 [10].

2. MAKO

- MAKO is a surgical robotic system developed by Stryker⁶ company. MAKO assists surgeon in performing hip and joint replacement surgery. It received the FDA approval in 2015 and started delivering market from the end of 2017 [54].



FIGURE 2.19: CARLO from Advanced Osteotomy Tools [12].



FIGURE 2.20: MAKO surgical robotic system [8].

3. Galen Robotic System

- Galen was developed at Johns Hopkins University by a PHD student and is commercialized by Galen robotics company. The robot reduces the surgeon tremors while operating and increases precision. It filters out the surgeon's hand tremors and avoid undesired motions [55].

4. DLR MIRO

- MIRO is a lightweight surgical robotic arm developed at DLR⁷ Institute of Robotics and Mechatronics. MIRO is a slim and a versatile robot arm aims for various existing and future medical robotic procedures. It assists the surgeon directly on the operating table [57].

5. Versius Surgical Robotic System

⁵KUKA, Augsburg, Bavaria, Germany

⁶Stryker, Kalamazoo, Michigan, U.S.A.

⁷German Aerospace Center, Cologne, Germany



FIGURE 2.21: Latest version of Galen surgical robot [56].



FIGURE 2.22: DLR Miro surgical robot arm [58].

- Versius is similar to the DLR's Miro surgical robot arm, it was developed by Cambridge Medical Robotics⁸ company. The surgical arm is designed to be flexible enough and have access to all surgical quadrants. The surgical arm was expected to come to market at end of 2018 as CEO of CMR Martin Frost mentioned [59].

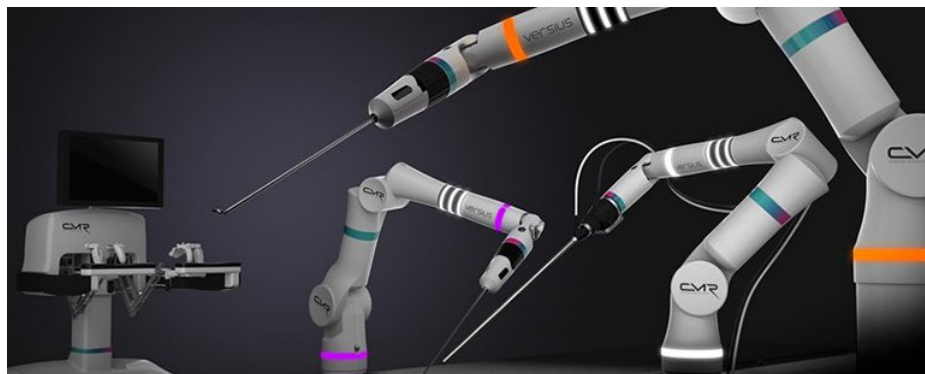


FIGURE 2.23: Versius surgical robotic system [60].

⁸CMR Surgical, Madingley, Cambridge, UK

6. I-SUR robotic platform

- The I-SUR (Intelligent surgical robot) robotic platform is a part of the European project I-SUR. The robot was developed at the ETH⁹ rehabilitation engineering lab. The robotic platform aims to increase the autonomy of surgical robotic systems in performing simple tasks, like suturing and puncturing [61]. It is based on a macro-micro robotic approach, where a two-arm micro-unit with hybrid kinematics is mounted to the end-effector of a larger macro-unit implemented as a linear delta robot as seen in the figure 2.24

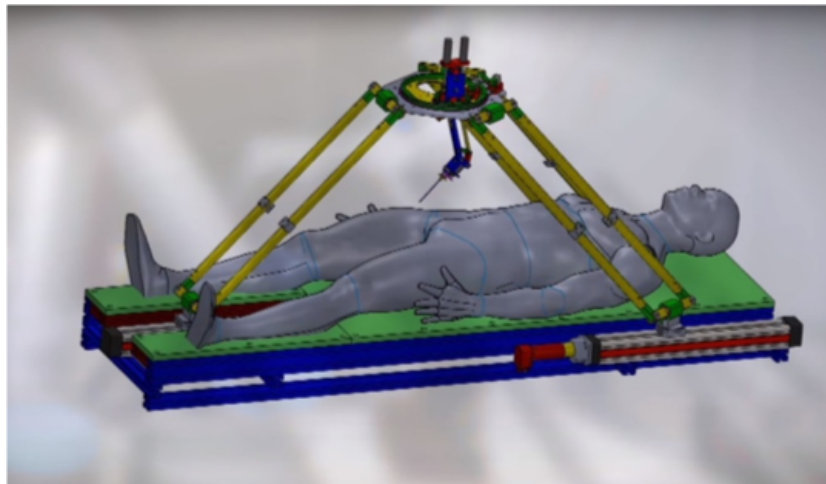


FIGURE 2.24: I-SUR robotic platform [62].

What we have seen above is some of the recent projects in the surgical robotic field aimed to assist in different procedures. Based on the designed mechanical structure, we realized that some of the robotic systems like CARLO and MAKO are still following the traditional positioning and mounting techniques used in the past. In which the robot system is mounted to a movable cart and placed in the working zone to perform the surgery. While, we can see other systems heading in a different direction. For example, MIRO and Versius robot arms operate directly on the operating table and can be relocated at any position when needed. Reducing the occupation zone needed for a movable cart beside the operating table. On the other hand, the I-SUR robotic platform is using the hybrid structure and also mounted directly to the operating table increasing the autonomy of the system and freeing more space.

Despite the many successful robotic applications in surgery, we have realized that most of these surgical robotic systems and arms share mainly two drawbacks. Firstly, the surgical systems are mounted to a movable cart which requires extra time in adjusting the cart

⁹Swiss Federal Institute of Technology in Zurich, Zurich, Switzerland

and the robotic system, extending the overall operation time. Secondly, limiting the working space for the surgeons around the operating table and staff, besides restricting the robot workspace.

2.4 GG-1 Robot

In this section, GG-1 robotic platform is introduced highlighting its main features and how it functions differently. The features of GG-1 were compared with other existing robotic arms developed for same purpose.

2.4.1 Current State

GG-1 is a serial robot anthropomorphically inspired from a human arm in the aspects of link length and joint arrangement. The structure consists of 7 DoF's (PR6), a prismatic joint as the base joint, moving parallel to the humans longitudinal axis and 6 rotational joints including the flexoscope (Fig. 2.25). The first two DoFs (P and R_1) define the movement in the coronal plane. The next three DoFs (R_2, R_3, R_4) determine the insertion points location and orientation in the coronal plane. The insertion point is used as an RCM (Remote Center of Motion) for intra body manipulation. R_5 and R_6 handle the orientation and tip bending of the flexible endoscope.

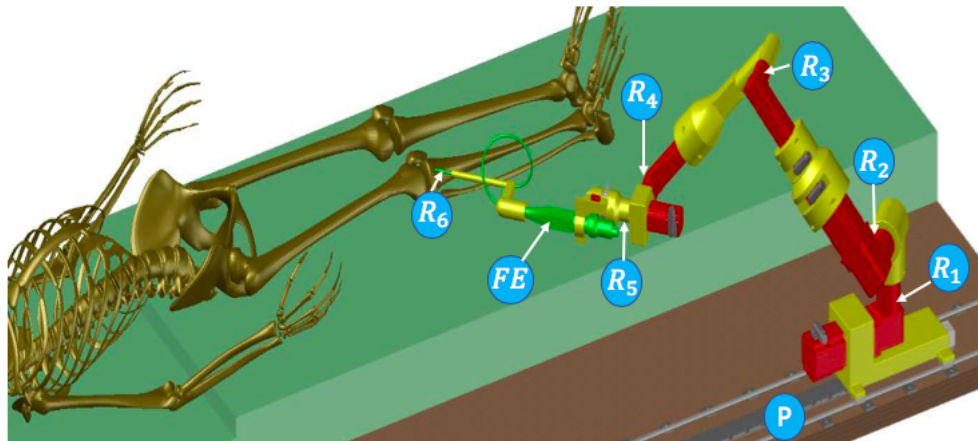


FIGURE 2.25: GG-1 platform CAD design.

The overall structure is built in 3D printed links connecting the joints (Electric motors) with an (commercial) intubation flexoscope mounted at the tip of the robot arm. The current platform was the first prototype of GG-1, in the next phases of the project, GG-1 will undergo variations in its architecture design. The components used for building the GG-1 platform are listed below.

- Magnetic linear servo motor (AL2412) for P joint, by Beckhoff Automation¹⁰(BA).
- Two DC servo motors (AM8131) with perpendicular shaft gearboxes (AG2250-WPLE60) for R_1 and R_2 , by BA.
- Two DC servo motors (AM8113) with perpendicular shaft gearboxes (AG2250-WPLE40) for R_3 and R_4 , by BA.
- A DC servo motor (AM8111) for joint R_5 , by BA.
- A Midi-servo (06.SW-0250MG) for R_6 joint, rotating the lever of the endoscope, by Savöx.
- Flexoscope (11301BND1) by Karl Storz¹¹.

An embedded PC (CX2020) with a single core Intel i3 processor are used for the control of the robot. Real-time transfer between motors and sensors is handled through the EtherCAT protocol at an update rate of 1kHz. Control is realized through Matlab/Simulink code compiled for TwinCAT3.

2.4.2 Robot Arm Features

The bio-inspired robot GG-1 has been developed to meet the requirements for orthopedic procedure in the knee. The flexible design makes it easier for redesigning the whole arm in terms of links and joints arrangement to adapt to other surgical interventions.

When looking at the intended use of other existing robotic arms in medical field and try to compare the main features regarding the joints arrangement, weight, payload and the maximum reach of the each arm. We realized that GG-1 robotic platform is not far from the standard designs in terms of mechanical structure, while the unique feature of GG-1 is the additional linear axis.

The table below illustrates the features of several robots commercially available and currently used in research. The robot arms were chosen for comparison due to the availability of specifications given from the manufacturer.

Firstly, starting with the number of degrees of freedom of each robot, we see that basically, only the GG1 robotic system is using the prismatic joint as a degree of freedom while all the others are composed of only rotational joints for maneuvering the robot arm. Regarding the weight, the current structure of GG-1 is approximately around 14 Kg and

¹⁰ Beckhoff Automation GmbH & Co. KG , Gtersloh , Germany

¹¹Karl Storz, Tuttlingen, Germany

Features	Dof	Weight	Payload	Arm reach length
KUKA	R7	25.5 Kg	7 Kg	1.266 m
UR3	R6	11 Kg	3 Kg	0.5 m
DLR MIRO	R7	10 Kg	3 Kg	1.1 m
GG-1	PR6	\approx 14 Kg	–	1.2 m

TABLE 2.2: Surgical robot arms features.



FIGURE 2.26: From left to the right: KUKA lbr Med 7 R 800 from KUKA (Germany), UR3 from Universal Robots (Denmark) and DLR MIRO from DLR (Germany) [63][64][58].

basically is the weight of the motors, gearboxes and the 3D printed links of the robot arm. The payload for GG-1 currently is the estimated weight of the endoscope ranging between 5 – 10 Kg which is close to the weight of given robot arms. The maximum reach of GG-1 from the base of the linear motor to the last rotational motor R5 (endoscope excluded) is approximately 1.2 meters, similar to the KUKA robot arm, also keeping in mind this maximum reach of the folded arm based on the arm links arrangement, where in our case still open for future redesigning.

It is shown from the comparison above that the design features of GG-1 first prototype is close to the standard design features of intended use of other robots in the operation room.

2.4.3 Robot Arm Mounting in Operating Room

Generally, operating room during an intervention is usually crowded. Devices and instruments are surrounding the operating table within the medical staff. The use of a robotic system to be located and mounted close to the operating table is a challenging task and has to be figured out in terms of space occupation and easy relocation.

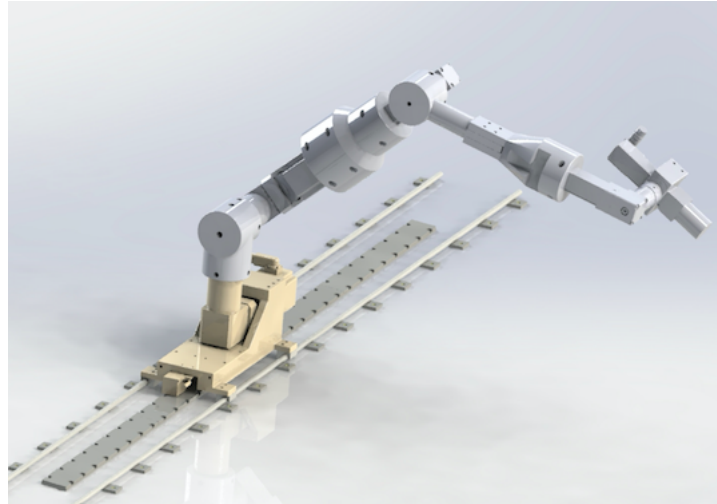


FIGURE 2.27: CAD design of GG-1 first prototype robotic platform.

The most common method for introducing the robotic system in the operating room is mounting it on a movable cart and placing the cart beside the operating table. For example, the da Vinci and ROBODOC robotic systems are mounted on a movable cart and adjusted close to the operating zone. In this way, it is easy to relocate the system when needed and put it away when not. The space occupied beside the operating table depends on the dimensions of the robotic system and arms workspace. Another option for mounting the robotic arm in the operating room is attaching the arm directly to the operating table. This idea started to spread recently with the new surgical robotic systems. For example, the DLR MIRO and Versius are two robotic systems consisting of independent robotic arms mounted directly to the operating table as we see in figure 2.28. This feature compared to the cart mounting option results in reduced space occupation around the operating table for the medical staff to move freely. Other options for locating the surgical robotic system in the operating room would be in the ceiling, on wall or mounted to the floor.

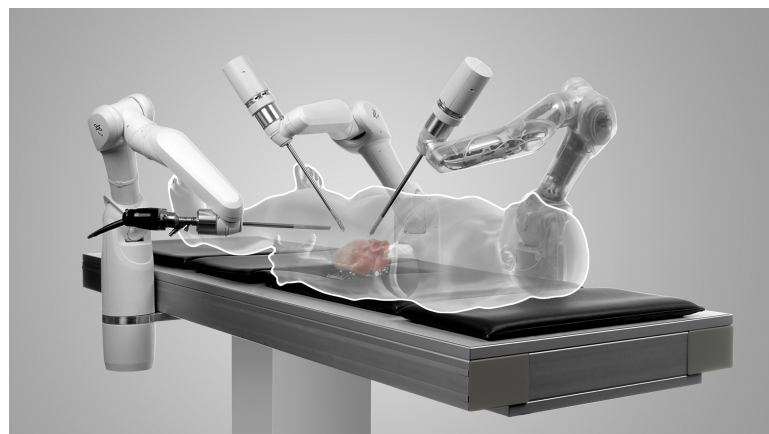


FIGURE 2.28: DLR Miro surgical robotic arms [66].

GG-1 for the moment is planned to be attached to the operating table directly, reducing the occupation space around the operating table, but still the concept of mounting the GG-1 under consideration and other options are still open and have to be reliably efficient for our application. Although these two mounting methods are commonly used nowadays, still a new concepts of mounting have to be tested and proved to share the operating room with the rest of the surgical robotic systems.

2.5 GG-1 Linear Axis System

In the industrial field the concept of using linear actuators or linear axis system is widely adopted. The main goal for using these linear actuators is to increase the workspace or the reach of the robotic arms in the industry and of course raise production rate and reduce the process time. Adding this linear axis to the robotic arm adds one DoF to the robotic system, giving it the possibility to move freely in one of the three translation axis (X,Y,Z). This innovative idea was used successfully in most of the industries and even for different applications (Fig. 2.29).

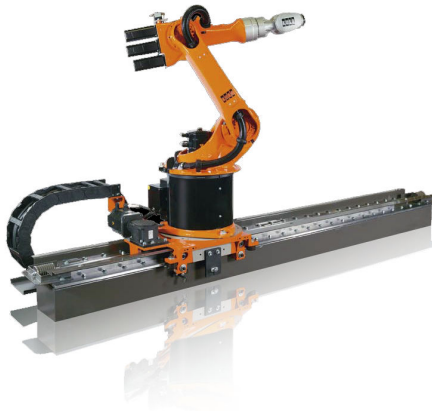


FIGURE 2.29: KUKA's Linear Unit [65].

This was inspirational to introduce this feature into the medical field and to use it for our GG-1 robot. For the same purpose the concept of adding a translation motion axis for GG-1 is to increase the workspace mainly. The workspace of robot manipulator is defined as the set of points that can be reached by its end effector [67]. In this way, our robotic arm is able to reach and cover most of the targets patients body in a semi-automated way. This transnational motion combined with the collaborative feature can solve the time consuming the other surgical robotic systems face, especially in a multi-site operations. For example, in some procedures like cartilage repair of joints, a graft has to be extracted from the patients body and implanted in the damaged part, and

this requires the robot to cut in two different sites in the patient's body [68]. This can be done simply by gripping the robotic arm and moving it to the new position in few seconds (Fig. 2.30). The time needed for adjusting the robot system to adapt to new operation for a new patient is undoubtedly shortened and is executed comfortably.

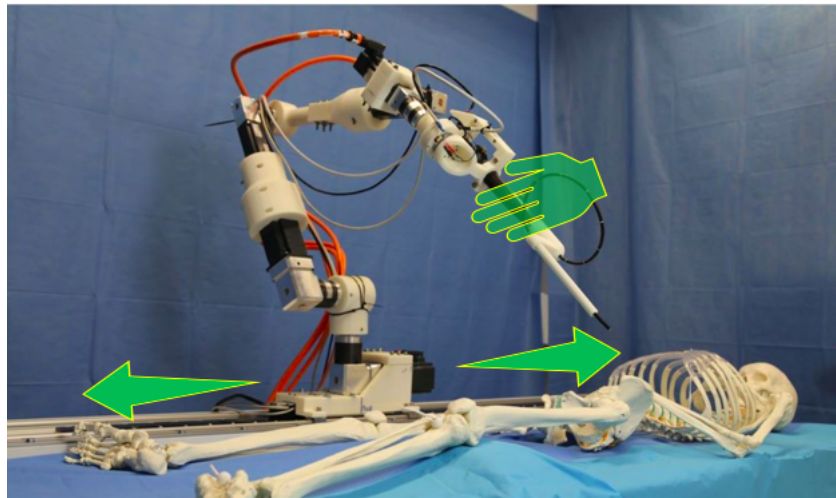


FIGURE 2.30: GG-1 collaborative feature.

One of the drawbacks of applying this concept in the operating room is hygiene and sterilization that are considered big challenges for our application environment. Adding technological equipment to the operating room might compromise the medical staff's ability to provide adequate infection control. Robotic systems usually are covered during the surgery to prevent any infections to transmit to the patient as shown in figure 2.31. Since the robot arm mounted to the cart of the linear axis must move freely along the rails, trying to cover the whole system is a challenging task. Adding a protective cover for the rails has to be done a way to guarantee the freely motion of the cart.

This concept has not been used by any of the current projects in research or developed previously by any company. Despite the mentioned challenges due to this additional axis, we wanted to evaluate it and proceed to see if this concept is a reasonable solution for our project and a reliable concept for future technology.



FIGURE 2.31: Surgical robotic system covered during surgery[69].

Chapter 3

Materials and Methods

This chapter presents the methods used for achieving the goal of the thesis. Starting with analyzing the current state of the linear axis system then defining the main requirements needed for the new design. Once the requirements defined, the next step is the redesign and assembly of the new system. After that, proceeding with controller tuning, system characterization and test movements performed for the new linear axis system.

3.1 Linear Axis System Main Components

A linear axis system is mainly composed of a drive train, guiding rails with bearings and a cart. In addition, a feedback system is used for tracking the position.

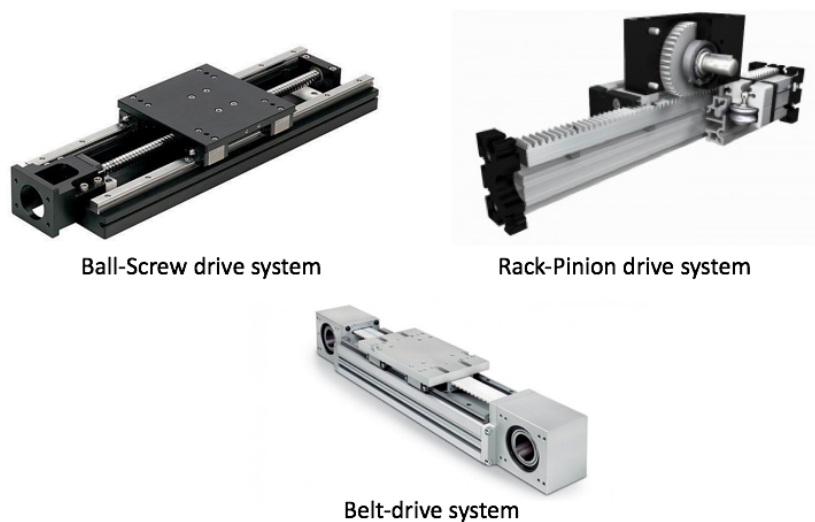


FIGURE 3.1: Linear axis systems existing mechanisms, Ball-Screw, Rack & Pinion and the Belt-Drive [70][71][72].

Many actuator styles and sizes are available, each with unique features suited to different applications and work environment. Common types of linear axis systems widely used nowadays are; the ball-screw drive systems, rack and pinion systems and belt-driven systems shown in the figure 3.1.

For the first prototype of the linear axis system a linear servo motor is used as a drive train. Two round aluminum shafts with plastic bearings are used as guiding rails and bearings respectively together with a 3D printed cart (Carriage) forming the base of the robot arm. The whole system is mounted on wooden base frame. The feedback system used is a Magnetic Encoder System (MES) from Beckhoff Automation. In the figure 3.2 we see the the list of main components of our linear axis system.

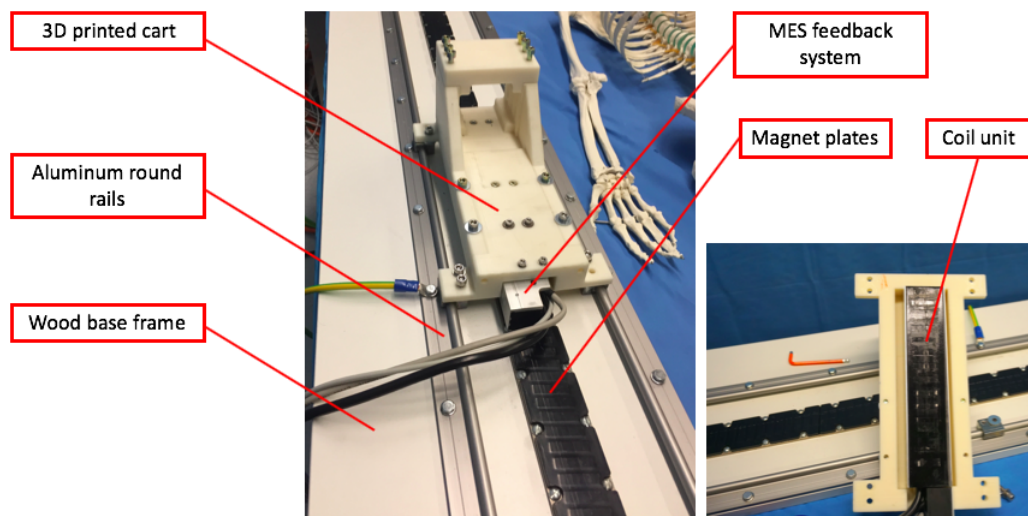


FIGURE 3.2: Linear axis system first prototype main components.

The linear servo motor has the same working principle of rotary motor, the rotational mechanism in the rotary motor is transformed into a flat mechanism. Consisting mainly of two parts, the primary and secondary corresponding to the coil unit and permanent magnet respectively. The primary is the moving part and the secondary is usually fixed on a frame as seen in the figure 3.3. The length of the magnet plates determine the reach of the linear motor. The linear motor has coils with an iron core, these cores that act like magnets are called the teeth (Fig. 3.4). The coils are supplied with a 3-phase electric current, by alternating the current phase of each coil the coil unit is propelled in one of the two directions based on the coupled phase with the magnet pole type (N or S). The speed of change in the current phase allows the control of velocity of the primary. In addition, the amperage of the current is linked to the moving force, yet increasing/decreasing the amperage allows control of the motor force.

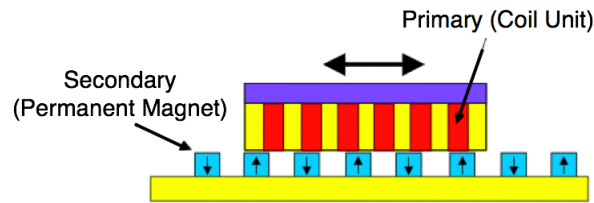


FIGURE 3.3: Linear servomotor main parts [73].

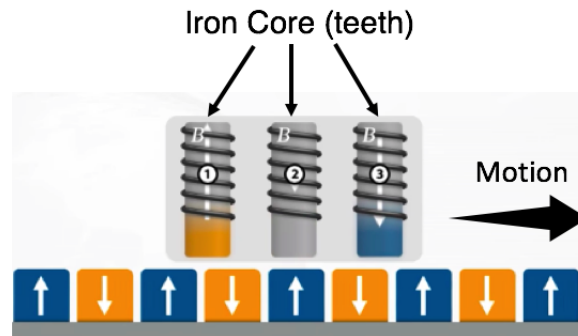


FIGURE 3.4: Linear servomotor working principle[74].

3.2 Current State Analysis

Before running the system and looking at the main defects in the structure, we observe a slight bending in the cart (Fig. 3.5) due to the fabricated material of the cart that fails to support the attraction force generated between the coil attached to the cart and the permanent magnet beneath (Fig. 3.6). The second defect of the system is a contact between the coil and the magnet that results in some scratches observed on the magnets when the system is running (Fig. 3.7). This contact is mainly due to the misalignment of the screws of slide bearings as seen in figure 3.8. In addition to these issues, no safety stops mounted for blocking the cart from accelerating and moving out of the operating range.

The round rails used are mounted on a wooden base frame, they are not aligned perfectly and can result in slight bending of the shafts due to the weight of the robot arm. Although, the system was running with all these defects with restrict velocity and limited movements of the arm. The last time we tried to run the linear axis it stuck and we were not able to move it any more (Fig. 3.9). At this point, the coil and magnets started to melt up when are in contact, this is due to heating effect of electric current flowing into the coil.

The feedback sensor used for the reading of the position of our cart along the rail is a Magnetic Encoder System (MES) from Beckhoff Automation (Fig. 3.10). A calibration

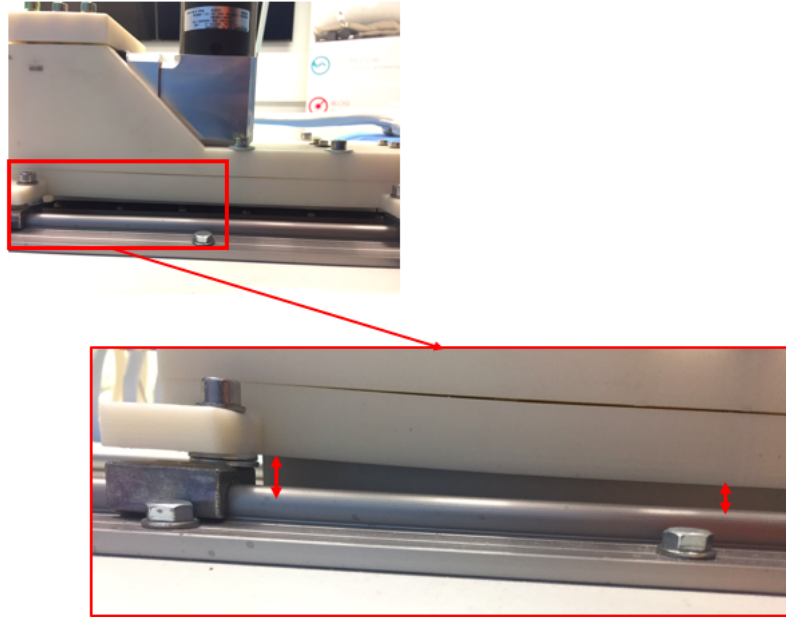


FIGURE 3.5: Carriage bending due to magnetic attraction force.

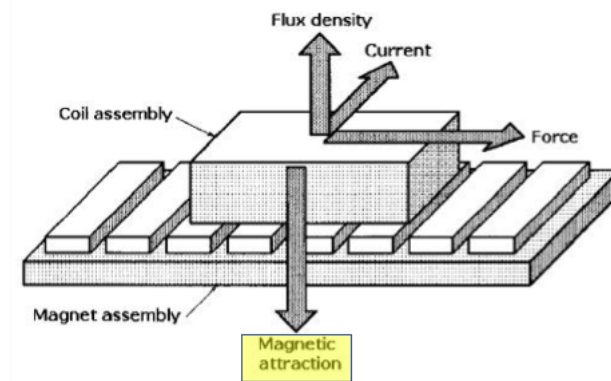


FIGURE 3.6: Magnetic attraction force generated between the coil unit and the permanent magnets [75].

is needed every time we run the system. In other words, the carriage of the linear system has to be placed at a starting reference point (defined as zero position) by the user in order to operate. The MES has a measuring resolution range of $5 - 10 \mu m$ and works directly on the magnets.

3.3 Definition of Requirements

Different mechanisms used normally for building a linear axis system. Based on the application's requirements in terms of velocity, rigidity and positioning accuracy, no single

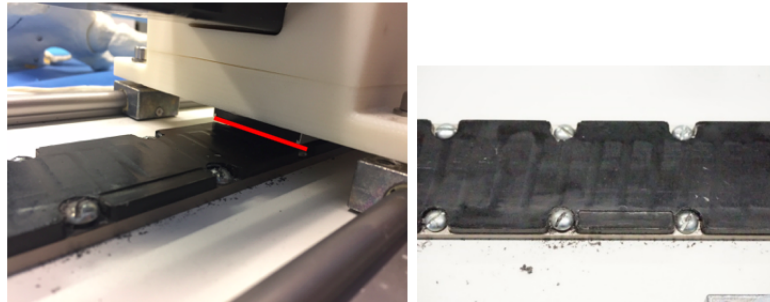


FIGURE 3.7: The direct contact between the coil unit and the permanent magnets and lack of the required air gap.

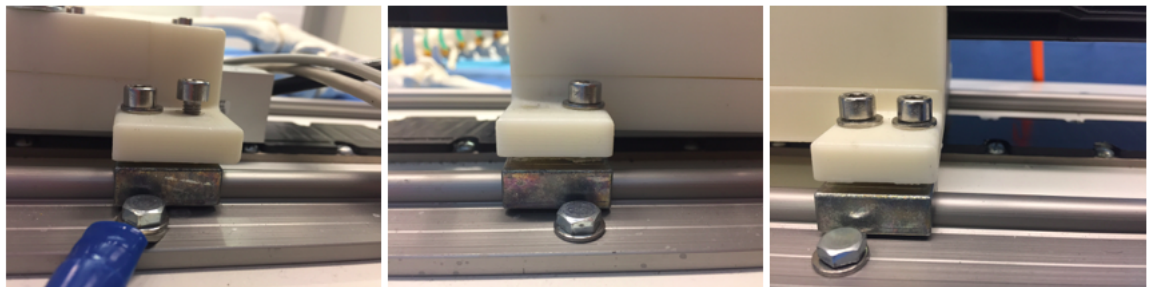


FIGURE 3.8: Misalignment of bearings screws.



FIGURE 3.9: Stacking zone of the coil part and magnets.

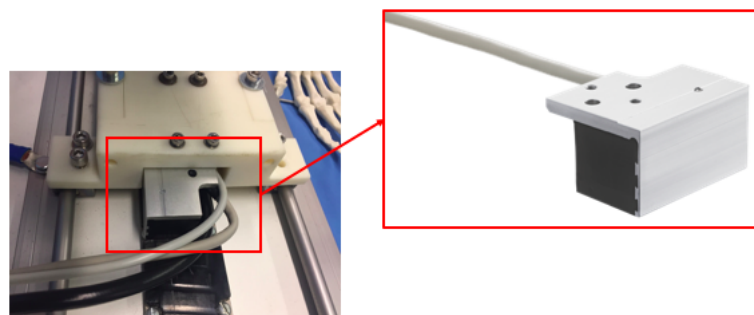


FIGURE 3.10: Magnetic Encoder System (MES) by Beckhoff Automation.

solution is optimal for every application. The mounting support and the mechanical design of the linear axis system can have direct impacts on the performance of the system. Each component reviewed separately below.

- **Drive train**

There are different types used for creating the linear motion. Ball-screws (Fig. 3.11) are often used as for linear motion applications like CNC machines, the use of recirculating ball bearings provides a high level of efficiency, load capacity and positioning accuracy. Lead-screws (Fig. 3.11) can deliver efficiency that comes close to ball screws on many applications, in addition they provide a high load capacity and very good positioning accuracy. The major difference between ball and lead screw is in load carrying between the moving surfaces. The ball screw uses recirculating ball bearings to minimize friction, while the lead screw depends on the coefficients of friction between the nut and the screw, which depends on the material used for both parts. Lead screws also offer many other advantages such as, more flexible configuration, quieter operation, ability to operate without lubricant keeping materials clean and of course the lower cost [76].

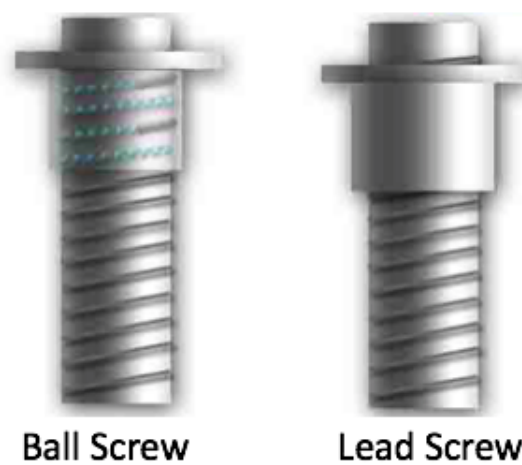


FIGURE 3.11: Ball and lead screw drive mechanisms [77].

The other existing drive trains used for linear actuators are belt drive and rack & pinions (Fig. 3.12). Belts and rack & pinions have several common benefits for the use in linear motion applications, they can provide high-speed travel over long lengths. Both are frequently used in large scale gantry systems for material handling, machining, welding and assembly. The belt drive is a loop of a flexible material used to link two shafts mechanically. On the driven end of the actuator (where the motor is attached) a precision-machined toothed pulley engages with the belt, while on the non-driven end, a flat pulley provides guidance [78]. In contrary, the rack & pinion mechanism consist of a rack "linear gear", a pinion "circular gear" and a gearbox. The gearbox helps to optimize the speed of the servo motor and the inertia match of the system. The tooth pitch and size of the pinion determines the maximum force that can be transmitted. Each of these systems provide some advantages regarding the stroke length, positioning accuracy, maintenance and setup environments. Both, belts as well as rack & pinions can hold very long travel lengths, while rack & pinion are not as precise as ball and lead screws, they do hold an advantage over belt drives in terms of positioning accuracy. While belt

systems do not require lubrication, the metal-on-metal contact of rack & pinion systems requires lubrication regularly. In harsh environments, belt driven actuators have an advantage because belts are hardly affected by contamination such as water or oil. Rack and pinion actuators, on the other hand, are open systems with no simple and effective way to enclose them, compared to belt driven ones that can be sealed completely.

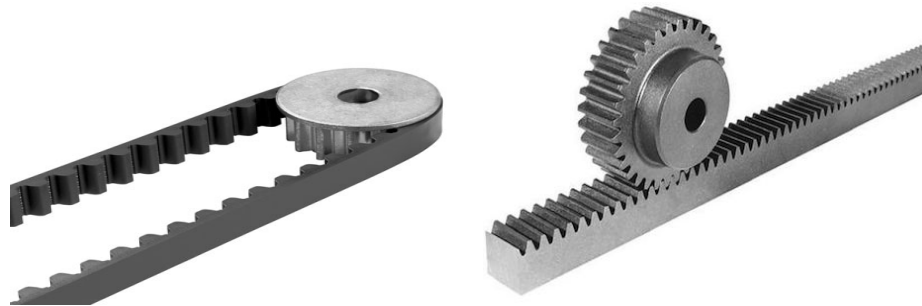


FIGURE 3.12: Belt drive (left) and Rack & Pinion (right) drive mechanisms [79][71].

The above types of drive train mechanisms have been commonly used for building a linear actuator or linear axis system. Based on the aimed application, the appropriate drive train is chosen. An additional drive train to be added to the category is the linear servo motor. The linear servo motor is a simple system made of two main parts, the primary containing electro-magnets and the secondary with either permanent magnets or magnet-free, as described in section 3.1. Linear servo motors offer high speed, acceleration, and precision with minimal backlash and settling times [80]. This is often one of the most costly technologies compared to the others. In the table 3.1 the different drive train mechanisms features are shown.

Comparing the different mechanisms we have in the table below, we notice that the linear servo motor has a maximum advantage of features among the other types of drive trains except the dirt resistance. It offers high accuracy in positioning and high rigidity. The mechanical contact-free design of the linear servo motor components results in a smooth and quite motion, as well as no maintenance needed like lubrication or pre-load adjustment for a long term. A drawback of this type of drive train is the lack of a protective cover or seal in case it is used in harsh environment.

- **Linear guides**

The second component reviewed for the linear axis system are the linear guides. Linear guides mainly come in two types, round and square. Choosing one over the other is not obvious because it depends on the application requirements. Round guides (Fig.

Features	Ball Screw	Lead Screw	Belt Drive	Rack and Pinion	Linear Servo Motor
Accuracy	Medium \approx 15 μm	Medium \approx 30 μm	Low \approx 250 μm	Low \approx 150 μm	High \approx 5 μm
Stiffness	Medium	Medium	Low	Low	High
Noise	High	Medium	High	High	Low
Maintenance	Medium (Lubrication)	Medium (Pre-load adjustment)	Medium (Belt tension)	High (Lubrication)	Low (None)
Dirt Resistance	Medium (Seal)	Medium (Sliding)	High (Harsh environment)	Medium (Jamming)	Low (Need cover)

TABLE 3.1: Table comparing the different drive train mechanisms for the linear axis system [81].



FIGURE 3.13: Round linear guide[82].

3.13) have been used for a long period and were expected to satisfy almost every linear motion-control situation.

Round rails are generally less expensive than the square rails and more forgiving in terms of misalignment, parallelism and moment loads. To attain a high accuracy of the round rails, they must be supported at both ends or at several points along their full length, similar to the round shaft used for the first prototype of the linear axis system. Moreover, the installation and maintenance for the round rails are easier and less expensive compared to the square rails [83].

On the other hand, the square or profile rails were initially designed for machine tool

industry. The square rails are stiffer and rigid, and their main advantage is their higher positioning accuracy, especially for milling and grinding machines. Also, square rails can support higher loads than round rails and can handle higher torques. To attain this level of accuracy, square linear guides require continuous support of its rails with high flatness and parallelism compared to the tolerances we have for the round guides.



FIGURE 3.14: Square linear guide [84].

- **Support and carriage**

Rigidity is a main requirement for linear axis systems. Normally, the guide rails have to be mounted to a rigid base frame to prevent any bending in the rails and maintain a smooth motion along the full length. The same for the cart or carriage, it has to be rigid to prevent any bending or mechanical defects. Additionally, to ensure the safety for the user, slide stops have to be installed at the edges of the rails to prevent the cart from sliding out causing harm to the user and damage to the system.

- **Position measuring system**

Two common types of linear encoders are frequently used for closing the control loop of a linear motion system: Magnetic linear encoder and optical linear encoder. Magnetic encoder have a band containing magnetic particles periodically magnetized north and south to form magnetic fields, and a read head that scans the magnetic fields. The output signals determine the direction and distance traveled along the axis. The optical-encoder technology uses a media such as steel tape or glass with fine graduations. When illuminated by a light source such as infrared LED or a laser, these graduations either reflect or pass light to a detector (Fig. 3.15). The size of the graduations determines the basic signal period. Mostly, graduation sizes vary from hundreds of microns to hundreds of nanometers [85].

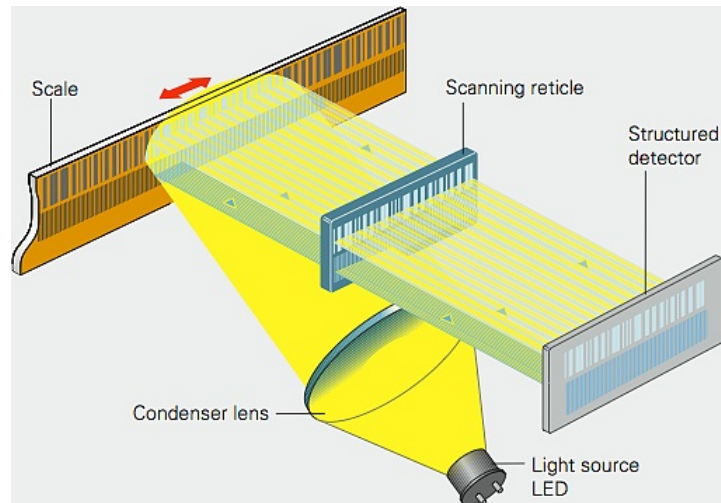


FIGURE 3.15: Optical encoder working principle [86].

Optical encoders come in two types of measuring methods incremental and absolute. With the incremental measuring method, the graduation consists of a periodic grating structure. The position information is obtained by counting the individual increments (measuring steps) from some point of origin. But, an absolute reference is required to determine positions.

In absolute method, systems provide unique position information from the moment they are switched on. Even movements that occur while the system is without power are translated into accurate position values once the encoder is powered up again. There is no need to move the carriage to find the reference mark. The absolute position information is read from the scale graduation which is formed from a serial absolute code structure.

- **Admittance control**

The last goal of the thesis is the implementation of the admittance control for the linear axis system. Admittance control is an approach to the control of dynamic interaction between a manipulator and its environment [87]. In our case the manipulator is the prismatic joint or the linear axis system. In robotics, admittance control defines the motions that result from an applied force. The applied forces are measured through Force/Torque (F/T) sensors. By utilizing measurements recorded by the F/T sensor these inputs of sensors are mapped into a velocity output signal for example (In velocity control mode) provoking motion of the system.

3.4 Solution Approach and Decision

Based on the reviewed components and our application requirements. The linear servo motor is a favorable drive train for our linear axis system. Smooth motion, high positioning accuracy and less dirt are main keys for our application in the operating room.

The linear axis system must support the robot arm in different poses where a torque can be created when the arm is extended. From the linear servo motor mechanical installation requirements, an air gap (< 0.5 mm) must be maintained between the coil unit and the permanent magnets during the motion. It is challenging to attain this tiny gap constantly along the entire rails using the round guides, for this reason a rigid linear guide like square guide is needed for our linear axis system to satisfy this requirement.

As seen before in figure 3.2, the system was mounted previously on a wooden base frame. This type of base frame is not a suitable solution to support the load and prevent bending of guide rails. To solve this issue, the wooden base frame has to be replaced with a stiffer material as aluminum for example to ensure flatness. The 3D-printed cart designed for the old system is not able to maintain the flatness of the coil unit with respect to the permanent magnets and also cannot resist the magnetic attraction force (≈ 900 N) formed between the two components, which results in unstable situation as seen in the in section 3.2.

Regarding the position measuring system, to eliminate the homing issue we have we must replace the MES with a full absolute linear encoder system. Different types of absolute encoders are available at the market each with different properties and advantages. The chosen absolute linear measuring system is LC 115 from HEIDENHAIN¹ (Fig. 3.16). The LC series from HEIDENHAIN is a sealed linear encoder mounted on a machined surface over the entire length. It has a measuring step of 10 nm compared to the (5–10 μ m) of the MES, offering the system the ability to move with small steps which is more likely needed for our application.



FIGURE 3.16: LC 115 absolute linear encoder system from HEIDENHAIN [88].

Our linear axis system has a single Dof and can freely move in both directions over the entire length of the rails. Therefore, one F/T sensor is required to measure the applied

¹Dr. Johannes Heidenhain GmbH, Traunreut, Germany

forces. The sensor has to be mounted at the top of the carriage to give the user the ability to move it freely.

3.4.1 Decision

The chosen components for building the new linear axis system are listed below.

- **Drive Train:** Linear servo motor (AL2024) from Beckhoff.
- **Linear guides:** Square linear guide rails with four ball bearings carriages (Linear Guide Rail PS 4-20) from Item24².
- **Support:** Aluminum profile frame (Profile 8 240x40) compatible with square rails from Item24.
- **Carriage:** Aluminum custom designed carriage.
- **Position measuring system:** Absolute linear encoder LC 115 from HEIDENHAIN.
- **Admittance control:** Force/Torque sensor (Mini45) from ATI³ mounted to a 3-D printed joystick.

3.5 Redesign

After the components were chosen, the CAD (Computer-Aided Design) drawing was designed in SolidWorks. The carriage newly redesigned in a way to be compatible with the linear servo motor and the linear rail bearing carriages, taking into account the main mechanical requirements for installing the two components of the linear servo motor (Fig. 3.17). Figure 3.18 shows the designed carriage where the coil unit has to be fixed from beneath with the MES adjacently with < 0.5 mm air gap in between. Four slide stops were designed to prevent the carriage from sliding out from the linear guides at both sides of the rails (Fig. 3.19).

The grinded aluminum base frame used make it easier for to mount the linear square guides aligned using T-nuts and screws for both rails and permanent magnets. The linear absolute encoder mounted to the side of the base frame and linked to the carriage through an aluminum side perpendicular angle part. An additional aluminum ruler was designed to sort out the cables of the linear servo motor, linear encoder, F/T sensor

²Item Industrietechnik GmbH, Germany

³ATI Industrial Automation, USA

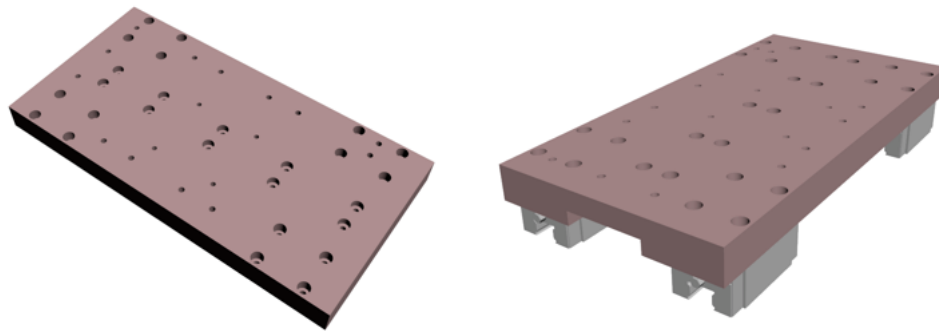


FIGURE 3.17: CAD design of the carriage.

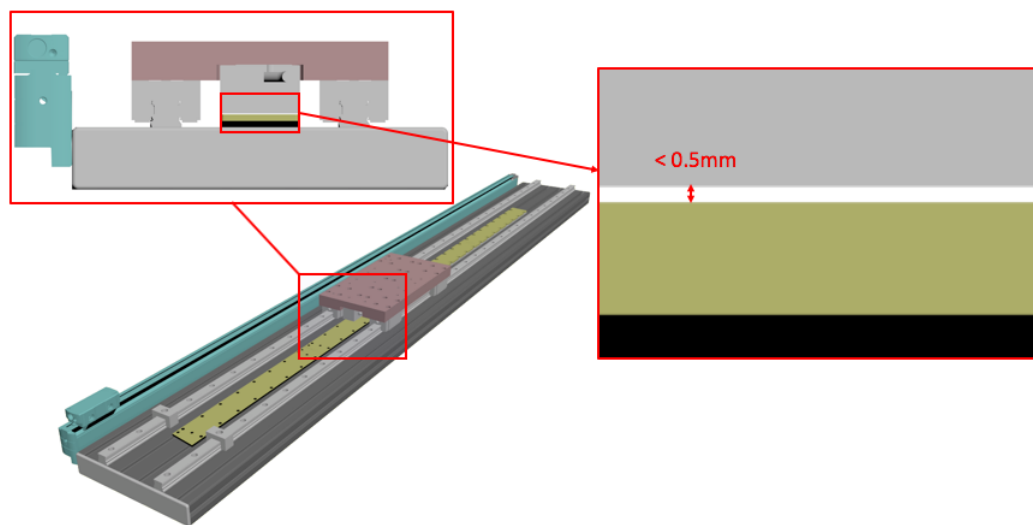


FIGURE 3.18: Figure showing the required air gap between the coil and unit.

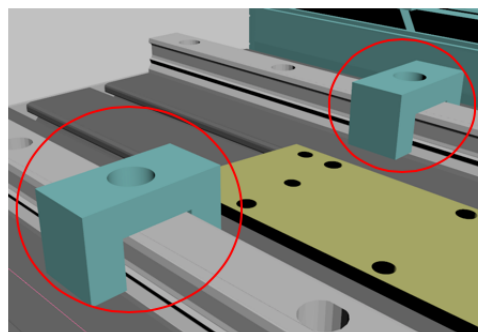


FIGURE 3.19: Slide stops CAD design.

and the robot arm motors cables later. For the robot arm to be mounted in the future, the mounting parts were designed also (Fig. 3.20). Four brackets with a flange for the horizontal motor to be mounted holding the whole robotic arm. In figures 3.21 and 3.22 the full CAD design of the new designed linear axis system and the CAD design of the entire robotic system are shown respectively.

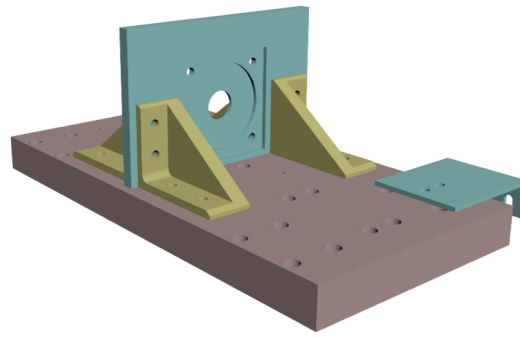


FIGURE 3.20: Robot arm mounting parts designed in SolidWorks.

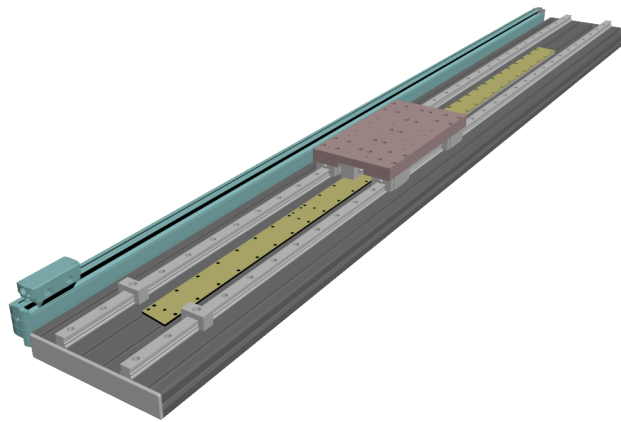


FIGURE 3.21: CAD design of full linear axis system.

3.6 System Setup and Commissioning

Once the designed parts are manufactured (Carriage, linking parts, slide stops, robotic arm mounting parts), the system components are installed according to the mechanical requirements of each. For example, the screws of the linear guide rails and unit coil are tightened with the required maximum torques 8 Nm and 5 Nm respectively. The magnet plates were assembled to the base frame and the carriage was mounted to the bearing carriages of the rails. After the full assembly of the system, the linear servo motor was connected to the linear drive AX5000. Plus, the absolute encoder connected to the linear drive via the optional encoder card AX5701 from Beckhoff (Fig. 3.23). The optional encoder card was used since the standard feedback inputs (X11 and X21) of the linear drive does not support the HAIDENHAIN interface connection "EnDat".

The maximum traveling range of the carriage was limited by the number of permanent magnets used. For our system, four permanent magnet plates were used of 384 mm length each (Fig. 3.24) resulting in a maximum travel length of the rails of 1.536 m.

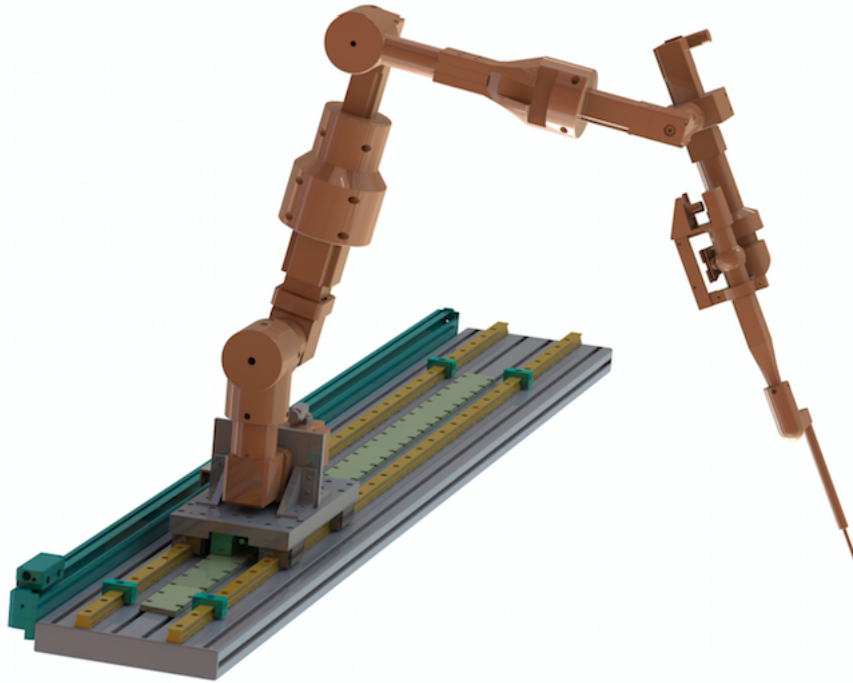


FIGURE 3.22: CAD design of the full robotic system.



FIGURE 3.23: Optional encoder card from Beckhoff [89].

The full assembly of the new developed linear axis system is shown in the figure 3.25 below.

Our linear axis system was controlled in real-time through TwinCAT3 automation software running on an embedded PC CX2020 from Beckhoff. The linear servo motor connected together with the feedback system to the servo drive AX5000 that communicates via EtherCAT with the embedded PC. For our system, the control scheme and parameters were defined in MATLAB⁴ and the model created in the graphical block diagramming tool Simulink. The Simulink model was compiled and the generated code was integrated into TwinCAT environment.

In TwinCAT drive manager (TCDM) (Fig. 3.26), the servo drive was configured where the type of motor and the feedback system were selected. A new Simulink model derived

⁴The MathWorks, Inc., Massachusetts, USA

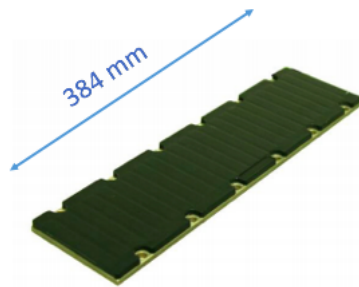


FIGURE 3.24: Single permanent magnet plate.

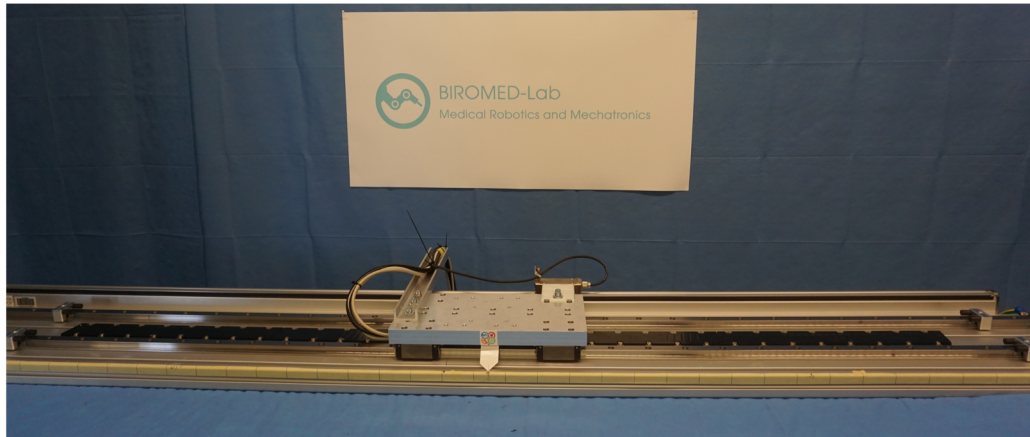


FIGURE 3.25: The new developed linear axis system full assembly.

from a previously existing one used for controlling the full robot was created separately with some variations in variables. For example, travel length of the carriage was limited to 0.5 m in both directions and maximum output speed of the linear motor was restricted to 0.25 m/s. The axis was limited to stop the carriage few centimeters before running out from the range of magnet plates and hitting the slide stops. On the other hand, limitation in speed was due to two factors. Firstly, in our application the surgeon will grab the full robot arm and move it freely to a desired position. Therefore, a smooth movement and robust control is required. To achieve that, no high speed or sudden movements was tolerated, which could cause any harm to both surgeon and patient. Secondly, the reason for limiting speed was to ensure safety for user during developing and testing the system where an unexpected movements of the linear system could cause serious damage and harm for the surrounding people.

Once the system was configured in TCDM and the Simulink model was tested and integrated into TwinCAT, the system was launched. The MES was configured first in the TCDM for commissioning. The phase sequence of our linear motor must match the counting direction of the MES. This was checked using the command P-0-0166 "Motor and feedback connection check" (Fig. 3.27). After clicking the start button, the

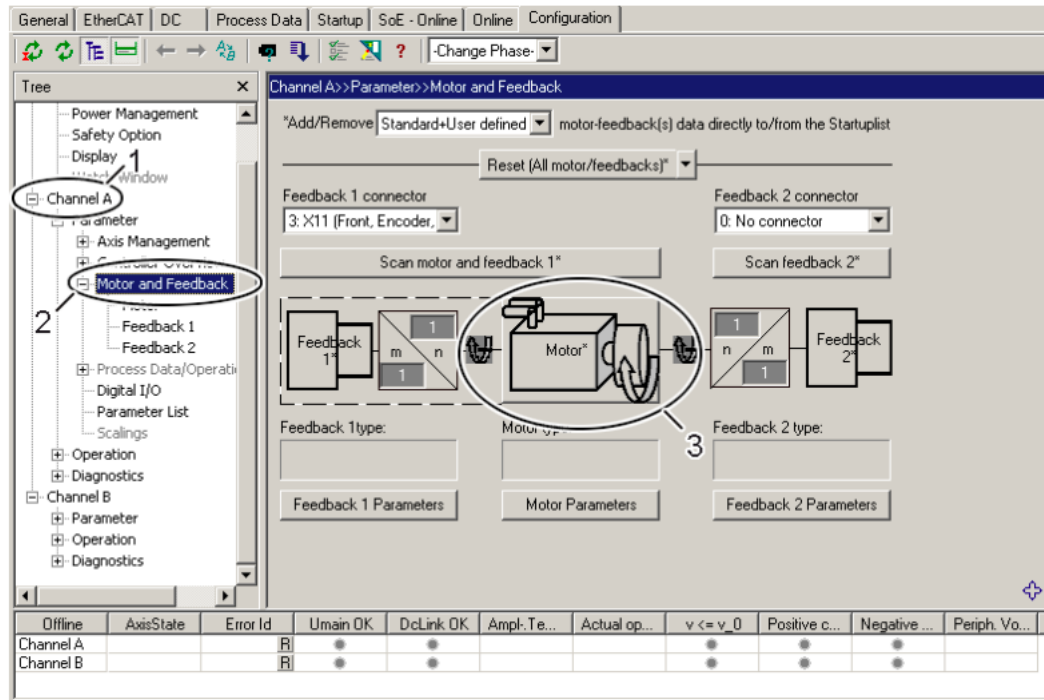


FIGURE 3.26: TwinCAT drive manager.

linear motor first jerks and then makes a further movement. Later, a message appeared "Succeeded to start the command" and a Yes was shown in the "Equal directions" command, meaning the successful execution of the command (Fig. 3.28). The next step recommended after the correct matching direction of the motor phase with our measuring system was the commutation offset. The value appeared in the commutation position difference (electrical) was subtracted from the initial P-0-0057 parameter "Electrical commutation offset" (270 or 90) and add 360 if the value was negative. Then this result was the new value for the P-0-0057 parameter "Electrical commutation offset" and had to be inserted in the "SetValue" and activated. The value was displayed in the setting "ActValue" after the download was completed. We executed the command P-0-0166 again and checked the value of "Commutation position difference". From the manual this value should now lie within the range (355 – 360) or (0 – 5) degrees. In our case the value was within the required range, meaning the commutation was executed successfully. The commutation was done on different positions along the linear axis and all results were in the range of 5 degrees.

After the execution of the commutation offset and synchronization of the counting direction of our measuring system with motor phase, the MES was replaced with the absolute linear encoder in the TCDM and tested for functionality. The system was tested with the default parameters of the linear drive controller. Since a new mechanical system was installed running with the old controller parameters the system did not perform properly. While testing, the system started releasing a disturbing loud noise. This indicated

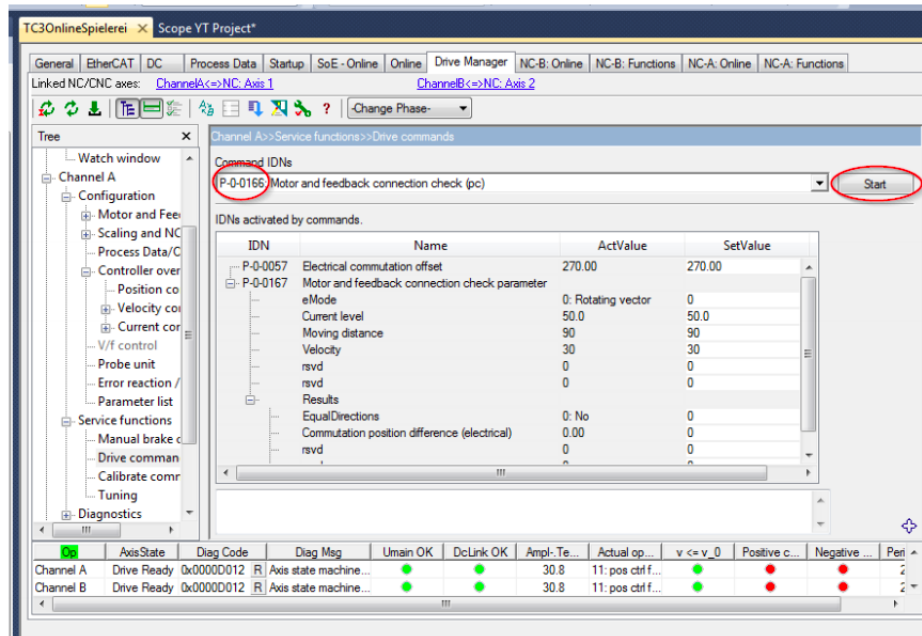


FIGURE 3.27: P-0-0166 command window in TwinCAT drive manager.

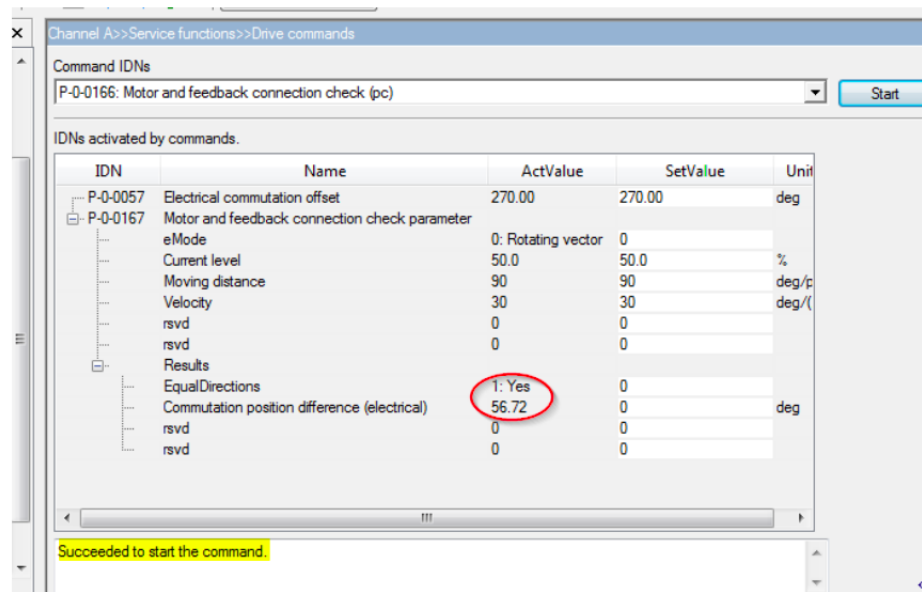


FIGURE 3.28: P-0-0166 command window in TwinCAT drive manager after execution.

that our controller had to be tuned again for our new linear axis. The control algorithm and control tuning method used will be described in the next section.

3.7 Controller Tuning

Friction and inertia can cause complex dynamic behaviour of a system. Therefore, a control algorithm is needed to ensure well-performing response for our system. In this

section an overview of the our system controller and tuning method are illustrated.

3.7.1 Controller Overview

A graphical representation of the control scheme of our system is shown in figure 3.29. We are dealing with a closed-loop control system because our feedback sensor is monitoring the position and feeding it back to our control system. At this point, the actual output signal is compared with the desired input signal. The main role of the controller is to reduce the measured difference in signals and bring it back to the original or set value. Generally, closed-loop systems are designed to automatically maintain the desired input by generating an error signal which is the difference between the input and output.

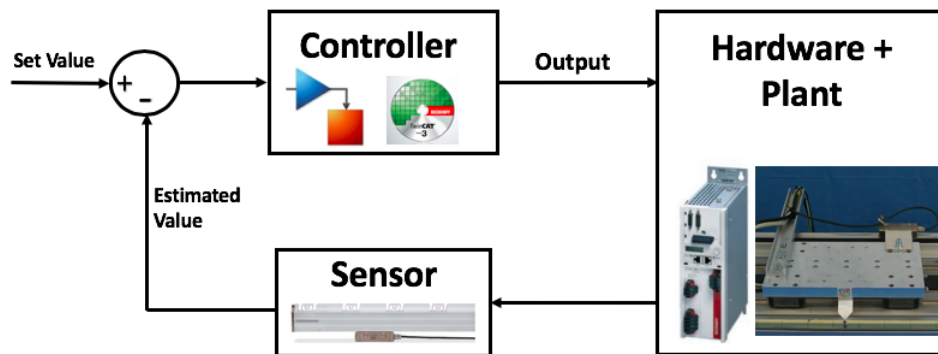


FIGURE 3.29: System closed-loop control representation.

The most commonly used control algorithm is the Proportional-Integral-Derivative (PID) controller. Due to its simplicity in implementation and its robust performance in wide range of conditions. The PID control algorithm is composed of three parameters or gains (K_c , K_i , K_d), each of these gains has its effect on the output signal of the controller. The influence of each term on the controller output is listed below.

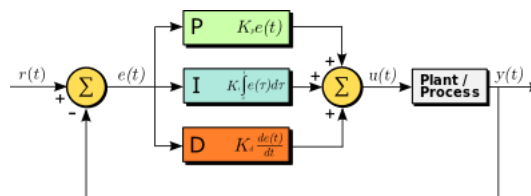


FIGURE 3.30: Parallel configuration of the PID controller [90].

- **Proportional gain:** K_c acts proportionally to the error signal $e(t)$. For example, if the error is large the control output will be proportionally large. In general, increasing the proportional gain will increase the speed of the control system response.

- **Integral gain:** The K_i sums the error term over time. It acts after the application of K_c to eliminate the residual error by adding a control effect due to the historic cumulative value of the error.
- **Derivative gain:** K_d estimates the future error $e(t)$ and gives additional control action when the error changes consistently. K_d reduces the effect of $e(t)$ by exerting control influence generated by the rate of error change [91].

The process in settling these gains is called tuning. The tuning parameters are derived from each control application. Although, different tuning methods are existing for our application we used *Ziegler-Nichols* tuning method [92].

Our controller was branched into two parts, low level controller, and high level controller as seen in figure 3.31. The low level controller was built-up on the servo drive of our linear servo motor, and configured initially by the manufacturer with default parameters. The second part was the high level controller to control the position command and ensure high position control of our system.

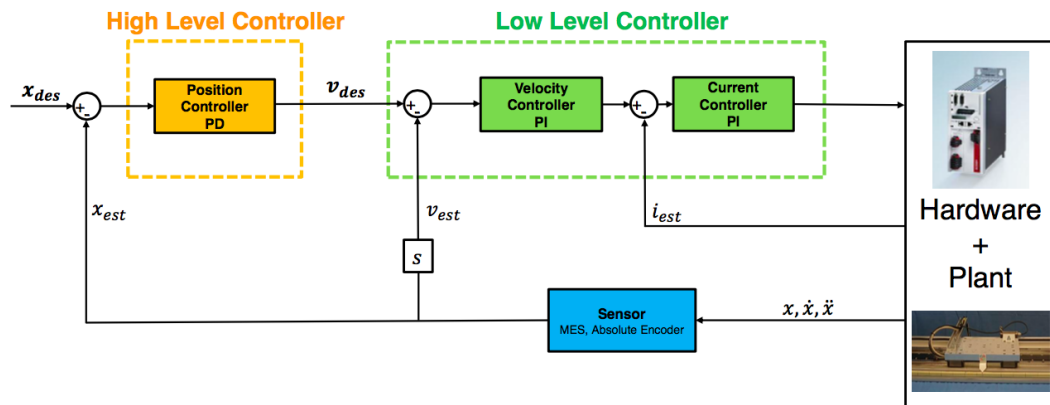


FIGURE 3.31: System controller overview.

3.7.2 Low level Controller

The servo motor drive controller consist of three types of control loops: a position loop, a velocity loop, and a current loop as shown in the figure 3.32. Depending on the application and performance requirements, the user can choose the control mode for his application. For our system, the velocity control loop was used in combination with the current loop, which in the cascade connection is nested inside the velocity loop. Both current and velocity controllers have a PI (Proportional-Integral) controller parameters. Our current controller was left with the parameters tuned by the manufacturer and our task was tuning the velocity controller parameters.

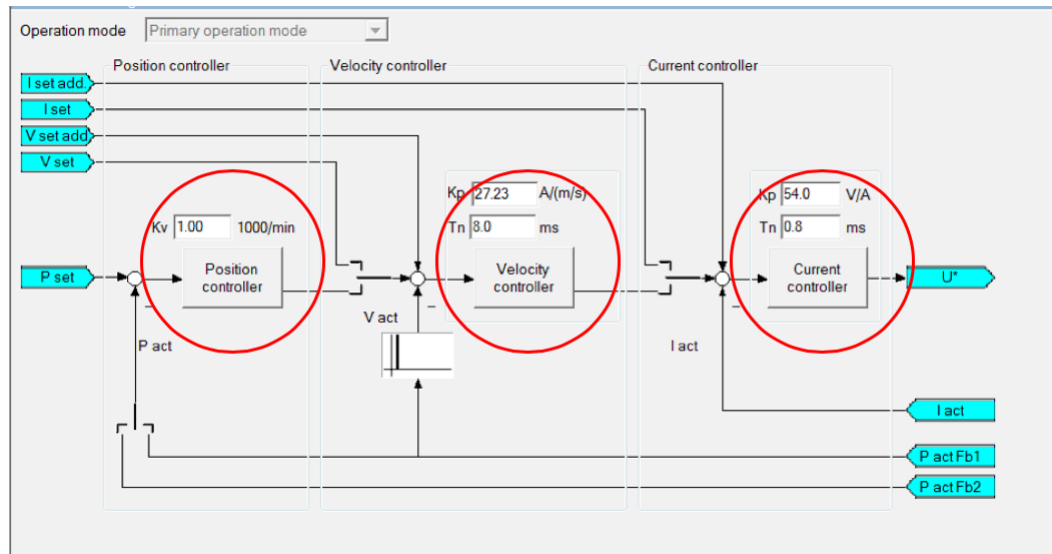


FIGURE 3.32: TwinCAT Control Drive Manager (TCDM) showing the three blocks of the controller.

The Ziegler-Nichols tuning method was used for tuning our velocity controller parameters. Since the proportional gain is the parameter mostly influencing the controller output and correcting proportionally the difference error of signals, it has to be tuned first. The Integral parameter was set to a very small value to reduce its effect on the output performance. According to Ziegler-Nichols tuning method, the aim is to find the critical value of the parameter K_c and obtain the oscillation period T_c of the output signal at K_c . Basically, the critical value (K_c) is the value at which the system starts to oscillate and at the edge of reaching instability with a disturbing noise released from the system. Once the K_c was found, we calculated our optimal values and configured them for our controller.

Ziegler-Nichols method			
Controller type	K_p	T_i	T_d
PI	$0.45K_c$	$T_c/1.2$	-
PD	$0.8K_c$	-	$T_c/8$

TABLE 3.2: Table of Ziegler-Nichols method showing the PI and PD type controllers [91].

In the equation 3.1 we see the general formula of the PID controller algorithm being $y(t)$ the output of the controller [93]. Basically, the integral time T_i is used instead of the integral gain K_i , since it has more physical meaning. In formula 3.3 we see that K_i

and T_i are respectively proportional. Increasing integral time makes the output respond slowly, which is opposite of the effect of increasing integral gain. For this reason, we set our integral time to a high value (30ms).

$$y(t) = K_p e(t) + K_i \int_0^t e(\tau) d\tau + K_d \frac{de(t)}{dt} \quad (3.1)$$

Equivalently,

$$y(t) = K_c \left[e(t) + \frac{1}{T_i} \int_0^t e(\tau) d\tau + T_d \frac{de(t)}{dt} \right] \quad (3.2)$$

where:

$$K_i = \frac{K_c}{T_i} \quad (3.3)$$

We started to increase slightly the the K_p gain to reach the condition of the critical value. To find the critical value, we gave the system a velocity set-value and observed the system performance. The desired velocity used for our linear axis is 0.05 m/s (Fig. 3.33). At a value of 185 of the proportional gain we observed a high disturbing noise released from the system when starting the motion. At this point, this value was considered our critical value of the proportional gain K_c . Using the table 3.2 we set the optimal value for the proportional gain $K_p=83$. Once the K_p was tuned we repeated the same procedure for the integral critical value. The critical value found for the integral time was $T_c = 6$ ms. Again from table 3.2, we calculated the optimal value to be set to our controller $T_i = 5$ ms. Based on the manufacturer manual for tuning parameters of linear servo drive, the minimum value of the integral time recommended is 5 ms the value which is the value we set for our controller. In figure 3.34 we see the tuned parameters inserted in the velocity controller block and configured in TCDM as the new controller values. At this point, the first part of controller tuning is accomplished. In the coming part we will see that the high level controller is more or less tuned in a similar way with minor differences.

3.7.3 High Level Controller

The high level controller was created by the user and developed in Matlab environment as a Simulink model (Fig. 3.35). This type of controller is less complicated than the low level in terms of control loops and tuning. This control loop was controlling the position command and comparing the feedback signal received from our absolute encoder directly

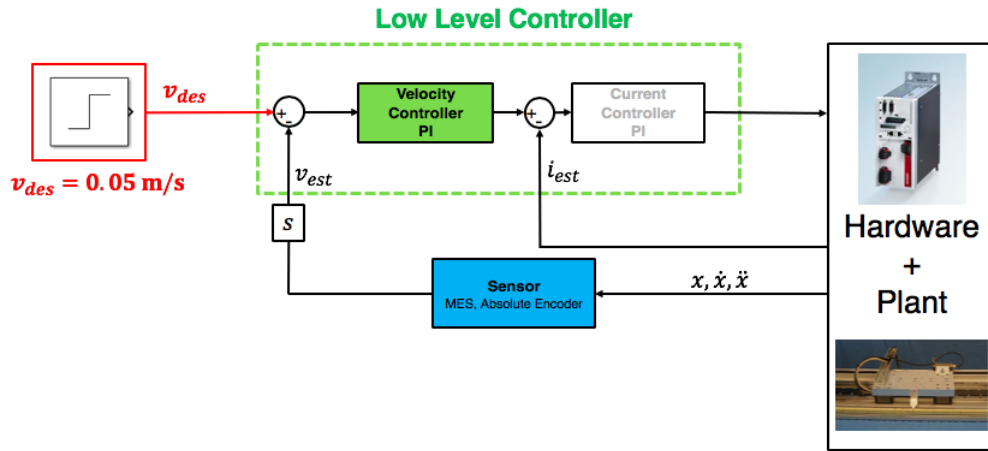


FIGURE 3.33: Velocity Input command.

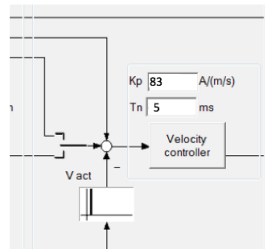


FIGURE 3.34: Velocity controller new parameters in TCDM.

with the desired input. A PD (Proportional-Derivative) controller type was applied to the error signal with a discrete-derivative block. Generating a velocity output signal since our system was in velocity control mode.

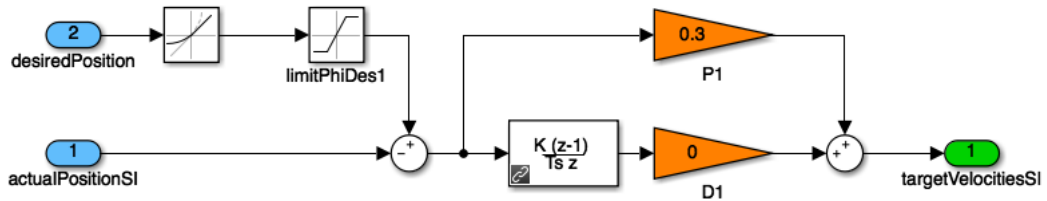


FIGURE 3.35: Simulink model of the high level controller.

We repeated the same procedure done in the low level to find the acceptable controller parameters. This time we generated a position command to our system. A sinusoidal wave signal was used with an amplitude $A = 0.3$ and a frequency $f = \frac{\pi}{4}$ (figure 3.36). We set firstly our derivative gain to zero and started tuning our proportional gain using Ziegler-Nichols method. We started increasing slowly the P gain and observe our system performance. The critical value found for K_p was 216, where the system started releasing a loud noise. From the table 3.2 we calculated the optimal value for P gain and set it to $K_p = 173$.

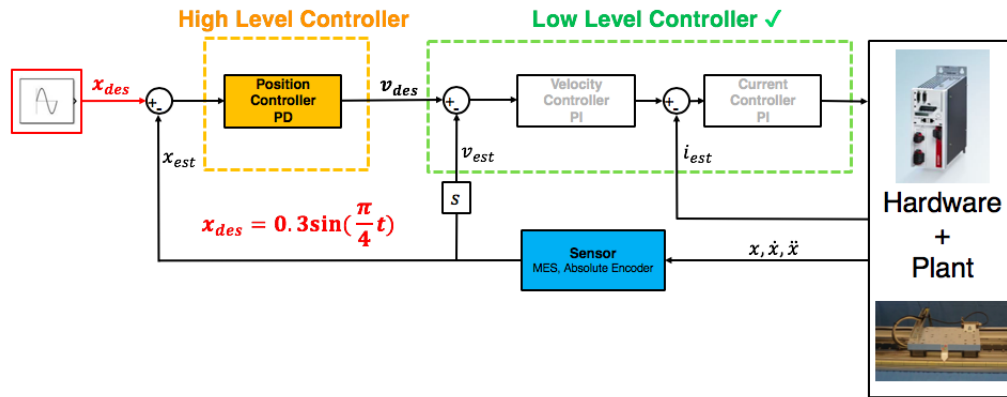


FIGURE 3.36: Graphical representation of high level parameters tuning.

Once the proportional gain was tuned, we tried to set-up an acceptable value for the derivative gain. We started increasing the derivative gain to reach an unstable condition of our system. The recorded critical value for K_{dc} was 0.022. Also, from the output signal at the critical value, we recorded the oscillation period $T_c = 25$ ms to be used for setting the value of derivative parameter from the formula $K_d = K_{dc}T_c$, the value inserted for K_d was 0.55. Also in this case the derivative time is used for tuning instead of derivative gain. From the table 3.2 the new value of derivative time is $T_d = 3.12$ ms.

At this point, the tuning procedure of our controller was terminated and the adjusted new values of our controller are shown in the table below 3.3.

Controller type	Low level control (PI)	High level control (PD)
K_p	83	173
T_i	5 ms	-
T_d	-	3.12 ms

TABLE 3.3: Table showing the tuned parameters of the new linear axis system overall controller.

3.8 System Characterization

Our system has a robust controller in which the tuning procedure was carried out through repetitive tests for obtaining the optimum parameters of the controller. The procedure was done with no load added to the carriage as seen in the figure 3.37. An additional load to the system will create an inertia and results in a variation of the system behaviour. Eventually, the controller is good enough and robust to the additional weight

and disturbance. System characterization helps us to observe how the system responds to input signals, through Bode plot and Step Response parameters.

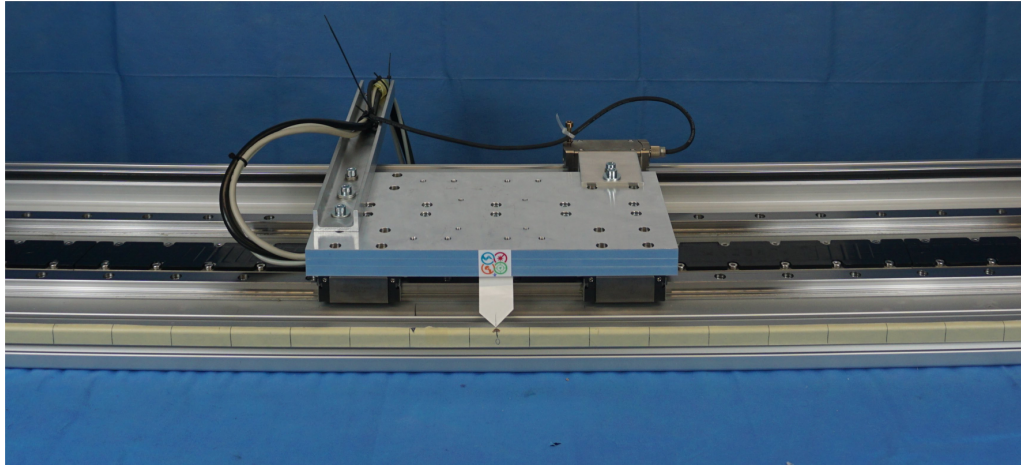


FIGURE 3.37: System state in tuning the controller parameters.

3.8.1 Bode Plot

Bode plot is a representation of the frequency response of our system. It consists of two parts, the first part showing the magnitude plot expressing the magnitude in decibels [dB], in the second part showing the Phase plot which is the phase shift in degrees [94]. Generally, when a system is subjected to a sinusoidal input with a given frequency the system responds at the same frequency with an output same or different to the amplitude of the input, with/without a phase shift in time.

In order to plot the frequency response and the phase shift, a sinusoidal input signal $x_{desired} = A_{in} \sin(\omega t)$ of a constant amplitude ($A_{in} = 0.5$ m) was applied in position control to our system. We varied the frequency (ω) of the input signal over time, and we recorded the output signal in the *scope* feature of TwinCAT environment for every single frequency applied. The applied frequencies for the plotting our bode plot are given in the table below 3.4.

ω [rad/s]	0.1	0.3	0.5	0.7	0.8	0.9	1.1	1.3	1.5

TABLE 3.4: Frequency values used for Bode Plot.

To plot the second part of the Bode plot, we calculated the phase shift and plotted it in function of frequency. To find the phase shift, the formula $\phi = \frac{\delta t 360}{T}$ was used. Being δ the time difference between the input and output signals and T the period of our sinusoidal signal.

3.8.2 Step Response

The step response represents output signal as function of time. The main parameters we usually look at to analyze in the step response are: *Rise time*, *Initial overshoot*, *Settling time*, and *Steady state error* as shown in the figure below.

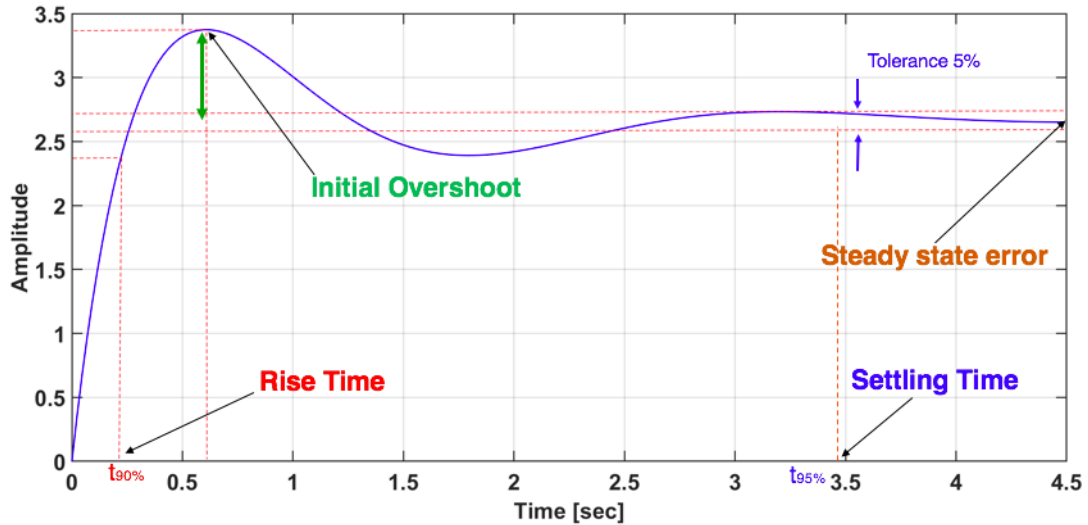


FIGURE 3.38: An example of a system step response demonstrating the main parameters of the step response to analyze.

- **Rise time:** is the time required to rise from 0 to 90 % of its final value.
- **Initial overshoot:** refers to the maximum value of the output minus the step value.
- **Settling time:** the time required for the response to reach and stay within a range about the desired value (in our case 5%).
- **Steady state error:** is the difference between the input and the output value of the system as time tends to infinity (in our case we defined it as the error after the signal has settled for 3s).

Every test was executed at steady state originating from zero position. The step response test was done on different step sizes ranging from 0.005 m to 0.5 m.

Step size [m]	0.005	0.01	0.1	0.2	0.3	0.4	0.5
---------------	-------	------	-----	-----	-----	-----	-----

TABLE 3.5: Step sizes chosen for plotting the step response.

3.9 Test Movements

3.9.1 Minimum Velocity

The first test performed for the new designed linear axis system was the minimum input velocity generated to our system and it still responds smoothly with no visible jerky movements. With the old system and MES feedback device, the minimum velocity we could reach was 0.01 m/s. This value was due to the resolution of the MES which was in the range of 5–10 μm and also dependent on the mechanical structure of the old system.

3.9.2 Demonstration Trajectory

In Matlab/Simulink environment a trajectory path model was created consisting of four main parts (Fig. 3.39). In the first part (green), a sinusoidal decayed sine wave was generated starting from an amplitude of 0.5 m and going down to complete 6 oscillations and return back to zero position.

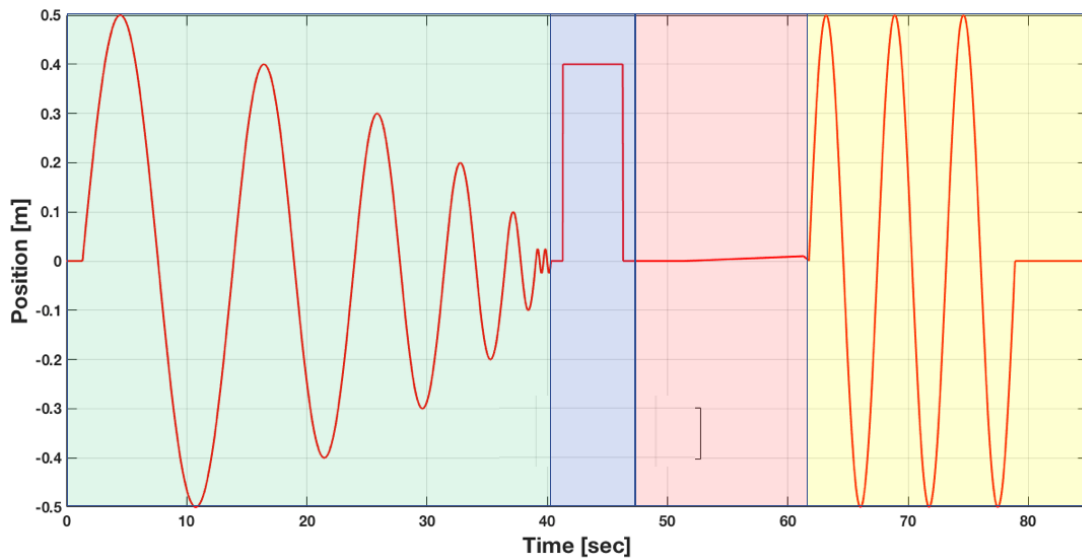


FIGURE 3.39: Demonstration trajectory consisting of four parts created for testing our system.

The position sine wave generated as input was $x(t) = A \sin \omega t$, where A is the maximum initial amplitude and ω is the maximum frequency. The maximum frequency is calculated from the given formulas:

$$x(t) = A \sin \omega t$$

deriving the equation to obtain the velocity:

$$\dot{x}(t) = \omega A \cos \omega t$$

where in our case,

$$\dot{x}(t)_{max} = 0.25 \text{ m/s, and } \cos \omega t_{max} = 1$$

then,

$$\omega_{max} = \frac{0.25}{A}, \text{ as } A = 0.5(1 - \text{decayRate}), \text{ with } \text{decayRate} = 0.2$$

Substituting the formula for the frequency $\omega = \frac{0.25}{A}$ with A decaying with time. Subsequently, the frequency ω increases with the same amount.

In the second part (blue) of our trajectory a step-up response of an amplitude of 0.4 m was given to our system at zero position and followed by a step-down response to return to zero again.

After reaching the zero position, the third part (red) of the trajectory was demonstrating the ability of the system to run at low velocity and follow exactly the desired input with a velocity 1×10^{-3} m/s.

In the last part (yellow) of the trajectory, a constant sinusoidal wave of an amplitude of 0.5m was given as an input with a frequency $\omega = 1.1$ rad/s, defined as the cut-off frequency for our system from the Bode plot.

3.9.3 Centered Weight

Although, in the demonstration trajectory we have seen the behaviour of the system with no weight added to the system, we had to test how the system will respond in loaded case. The robot arm has to be mounted to the carriage in the next step of the project. Accordingly, we tried to test the system reaction to a weight of 25 Kg, which is the estimated weight of the robot arm including payload. The system was tested with only one case, centered weight (Fig. 3.40). The performed test was executed with a velocity input of a value of 1×10^{-2} m/s within a distance of 25 cm.

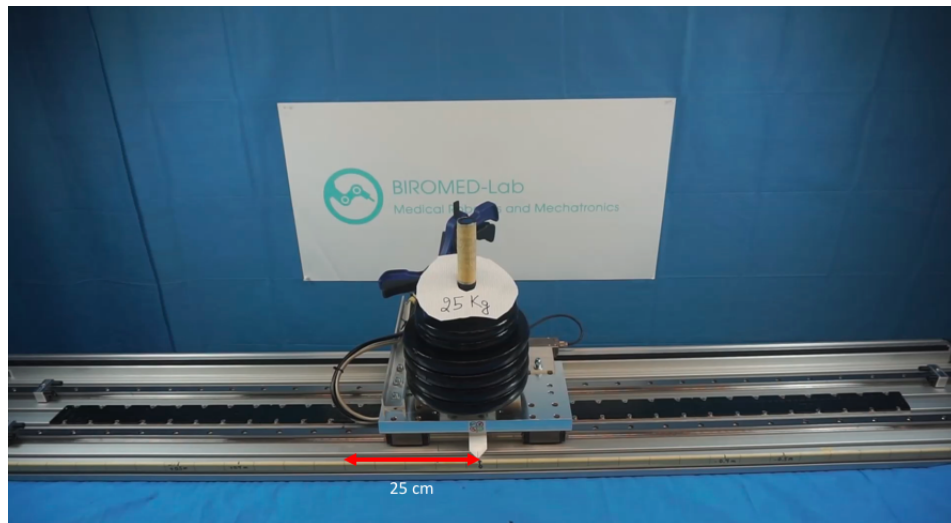


FIGURE 3.40: Centered weight of 25 Kg for testing system performance.

3.10 Admittance Control Setup

A Force/Torque sensor (Mini45 from ATI) was used to measure the applied forces from the user. The sensor was mounted to the base of a 3D printed joystick giving the user a high level in controlling the motion applied (Fig. 3.41). The sensor was connected via EtherCAT cable to the control cabinet and defined in TwinCAT environment as an input signal to be used in the control algorithm.

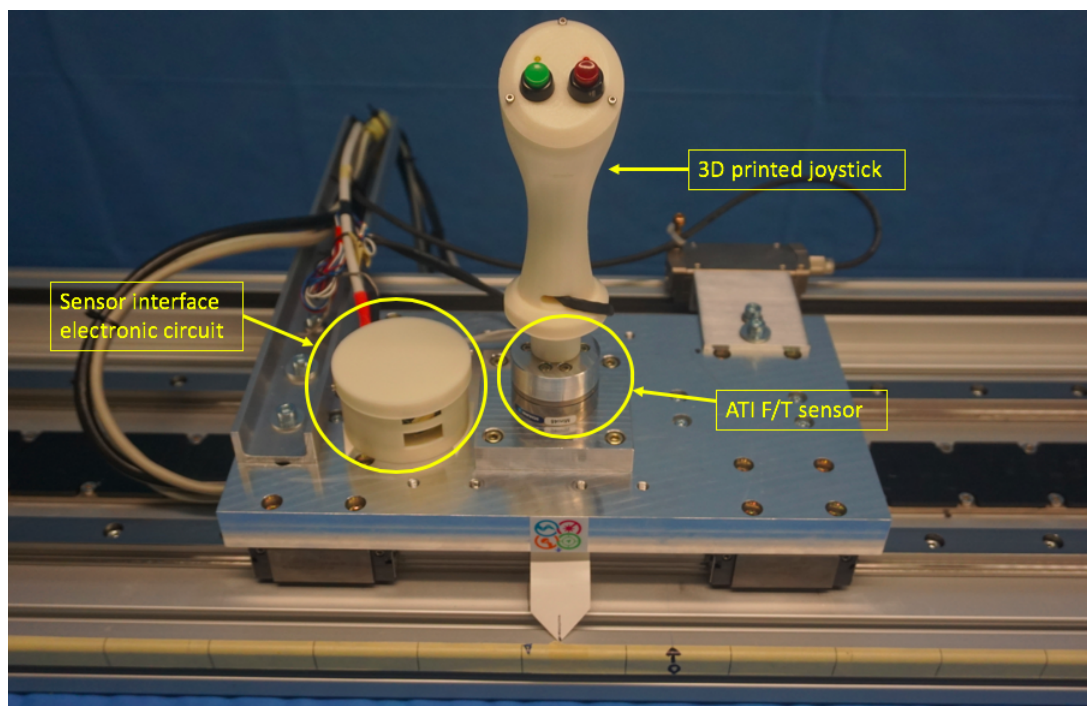


FIGURE 3.41: Admittance control setup.

A simple control algorithm was created for controlling the output speed relative to the applied forces. In the Simulink model below 3.42, the first part of the Simulink model was receiving directly the force signal from the sensor in [counts/N]. This value was converted to a force in [N] by multiplying it with 10^{-6} (From specifications of the sensor). The obtained force value in [N] was then provided to the second part of control algorithm as an actual input force.

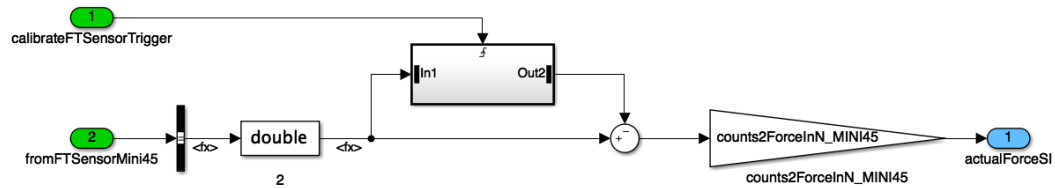


FIGURE 3.42: First part of the simulink model for admittance control.

In a second part of the simulink model (Fig. 3.43), the actual force (applied Force) signal in [N] was firstly limited to 5N. In other words, applied forces outside the range $[-5N, +5N]$ will not produce a higher velocity and the system will move with the settled maximum velocity only. Following the limit applied force block, a dead zone limit block has been implemented to limit the minimum applied force within the range of $[-0.1N, +0.1N]$. Resulting in zero outputs for inputs within this dead zone. Based on the relation we have between the force and the velocity $V = FP$, a proportional gain (P) is needed to attain a velocity as an output of our model. This proportional gain has to be tuned and built upon the user desire. A value of 0.15 was applied as P gain for our controller. In the last block, the output velocity was limited again to the value of $0.25m/s$ in both directions of the axis.

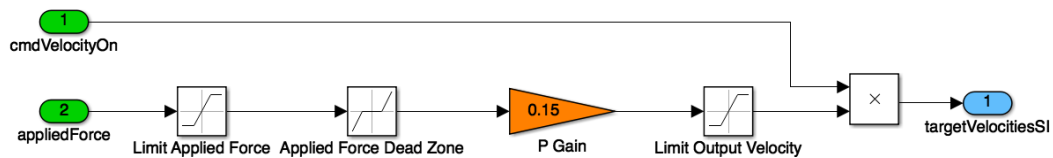


FIGURE 3.43: Second part of the simulink model for admittance control.

3.10.1 Evaluation Test

After the full setup and for the admittance control test and the developed algorithm, two evaluation tests were performed, OFF and ON modes. The two tests needed to observe the outcome of the admittance control approach. In the OFF mode, we tried to move the carriage along the entire rail to see the smoothness and have a feedback

of motion in absence of the admittance control (Fig. 3.44). In the second test (ON mode), we activated the admittance control model designed for driving the system and by grabbing the joystick and tried to move the carriage slowly to observe the difference in performance compared to OFF mode.

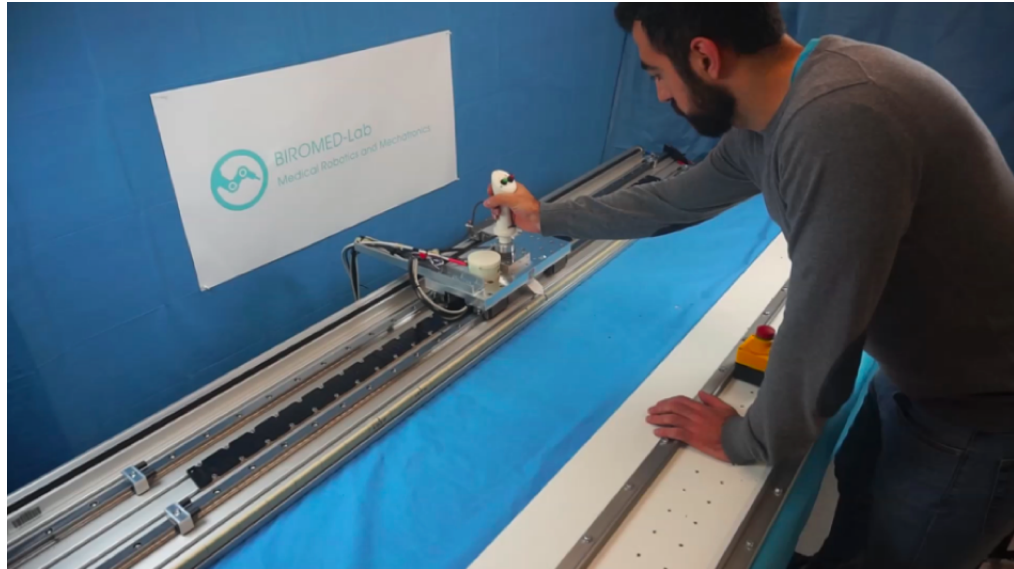


FIGURE 3.44: Admittance control evaluation test.

Chapter 4

Results and Discussion

In this chapter the results of system characterization and the performed test movements are presented and discussed briefly.

4.1 Bode Plot

The applied frequencies and the output signal's amplitude at each frequency are shown in the table 4.1. Also, the oscillation time of the output signal with the time shift between Input and Output signals are shown in the table.

ω [rad/s]	0.1	0.3	0.5	0.7	0.8	0.9	1.1	1.3	1.5
A_{out} [m]	0.5	0.5	0.5	0.5	0.47	0.43	0.35	0.3	0.25
δt [s]	0	0	0.114	0.301	0.45	0.894	0.726	0.723	0.711
T [s]	62.866	20.943	12.533	8.971	7.86	7.853	5.719	4.847	4.189

TABLE 4.1: Bode plot recorded data, ω is the frequency used for our plot, A_{out} is the output amplitude of the sine signals in meters, δt is the time shift between the Input and output signals in ms, and T is the oscillation period of the output signal in ms.

In order to plot the magnitude as function of the frequency, we computed the ratio given by the output amplitude A_{out} to the Input Amplitude A_{in} , and then applied the logarithmic function to the calculated ratio to obtain the magnitude in dB, $Magnitude_{dB} = 20 \log \frac{A_{out}}{A_{in}}$. Once the magnitude was obtained in dB, the first part of Bode plot was plotted (Fig. 4.1). The frequencies (0.1 rad/s to 0.7 rad/s) showed no variations in the output amplitude while the rest of the frequencies showed a decay in amplitude and increase in the time shift between the signals.

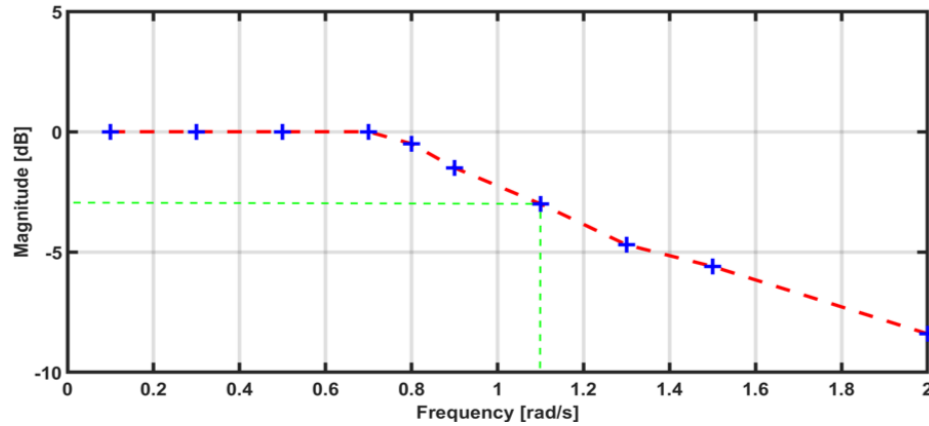


FIGURE 4.1: Magnitude plot.

Using the data from the table, we calculated the phase shift (in deg) at each frequency for the system and we plotted the phase part of our Bode plot (Fig. 4.2).

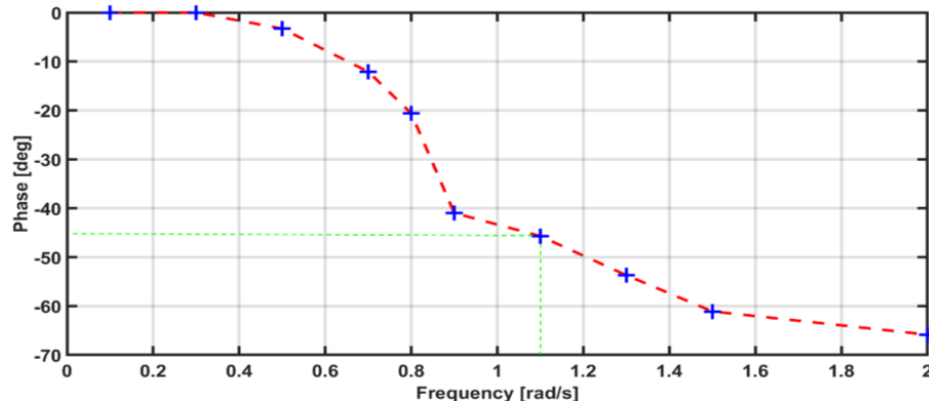


FIGURE 4.2: Phase Plot.

From the bode plot figures, we identified an important characteristic for our system, the cut-off frequency. The cut-off frequency defined as the frequency at which the ratio $\left[\frac{Out}{In}\right]$ is equal -3 dB in magnitude. At this point, the amount of attenuation started to increase rapidly as seen in both plots. The -3 dB loss in magnitude corresponds to a phase shift about 45 degrees where the system failed to follow the desired input signal. The zone before this point is defined as the bandwidth of system where the system can operate properly. From the above plots we realized that the cut-off frequency had a value of 1.1 rad/s. The characterization procedure was performed with the restriction in velocity we had set at the beginning in controlling our system. Meaning that the results of the bode plot were based on the defined velocity limit ($v = 0.25$ m/s) as a maximum output velocity of our control system. Once this limitation has been changed, a new characterization was needed. For example, if the maximum velocity output was increased the cut-off frequency with the same amplitude used for our tests ($A_{in} = 0.5$ m) would have increased.

The Bode plot was not defined previously for the initial prototype. But with these results and information we obtained regarding the bandwidth, we provided the user with the system working bandwidth which is an important characteristic to better understand our system state.

4.2 Step Response

Table 4.2 shows the results of the executed tests. The four parameters at each step were plotted separately using Matlab as shown in the figures 4.3, 4.4, 4.5 and 4.6.

Step size [m]	0.005	0.01	0.1	0.2	0.3	0.4	0.5
Rise time [sec]	0.027	0.045	0.369	0.729	1.089	1.449	1.809
Initial overshoot [10^{-4} m]	3.34	3.29	3.10	3.07	3.10	3.22	3.24
Settling time [s]	0.037	0.047	0.389	0.769	1.149	1.529	1.909
Steady state error [10^{-8} m]	-1.52	-0.762	3.81	3.05	0	-3.05	-10.68

TABLE 4.2: Results of the step response test done at different step sizes.

In figure 4.3, the rise time is increasing linearly with the increment of the step size. With the limitations settled to our system for output velocity, the time taken for every step to launch from steady state to the 90% of the final value will increase relatively.

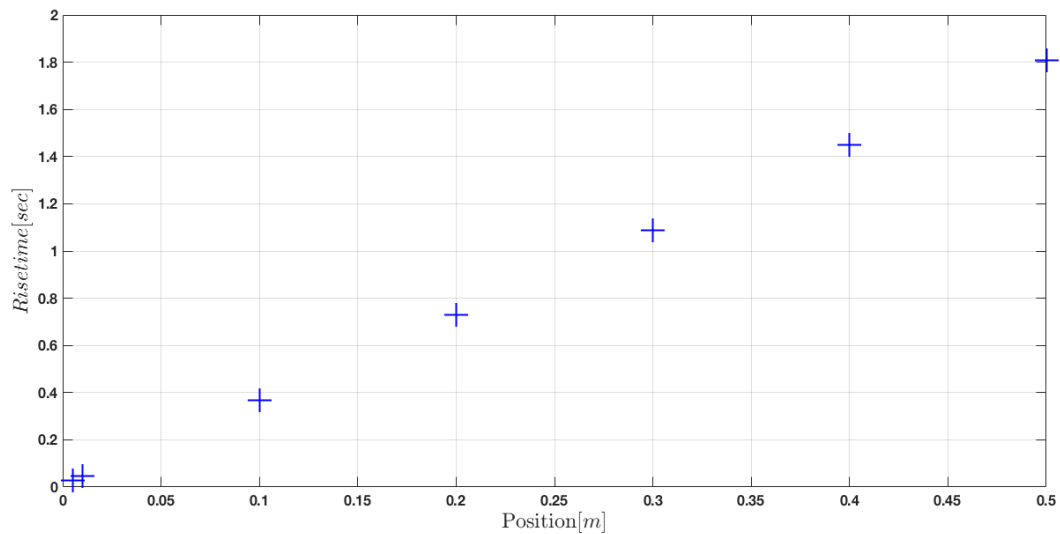


FIGURE 4.3: Rise time results.

In figure 4.4 the maximum initial over shoot was reported for every step. At 0.005 m step size the overshoot reached a value of 3.3410^{-4} m (6.68%), while for the rest of step

sizes it varied between 3.2910^{-4} m and 3.0710^{-4} m. The overshoot values obtained are acceptable compared to the step sizes we used in our test with 6.68% as a maximum reached with the smallest step.

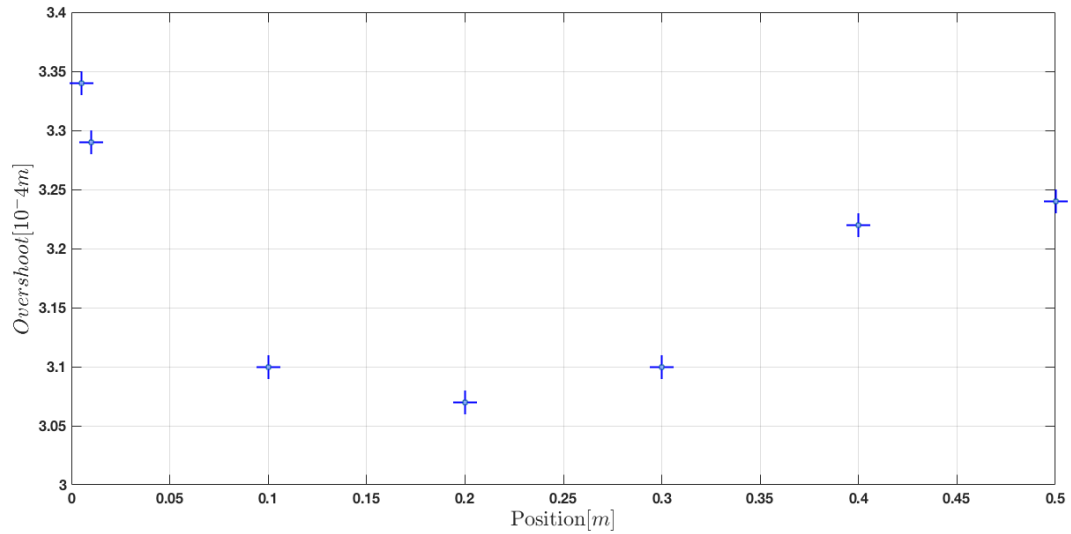


FIGURE 4.4: Overshoot results.

The results of the settling time (Fig. 4.5) are graphically similar to the rise time. From the graph we see the settling time increasing linearly with the increment of steps which is due to the velocity limitation of our system.

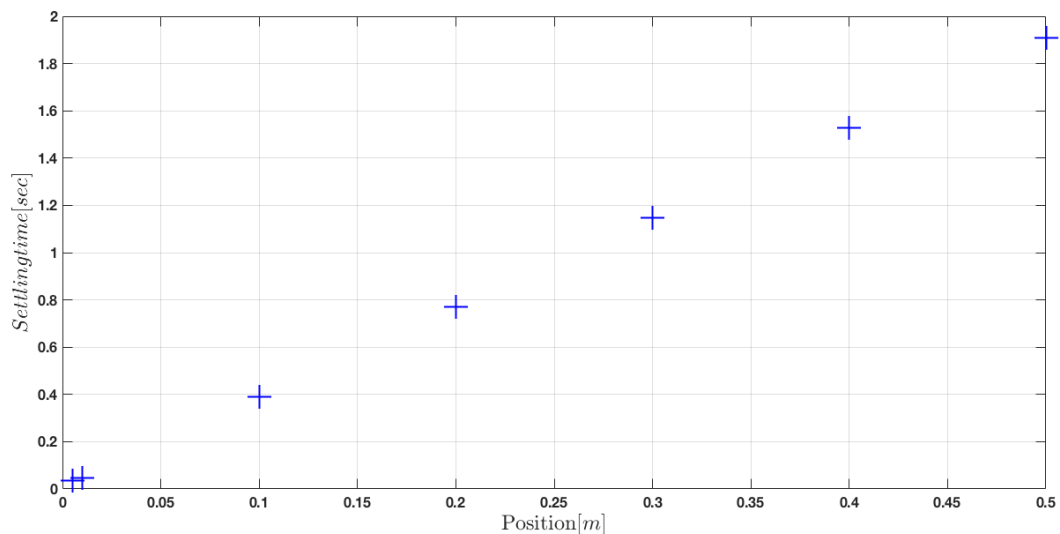


FIGURE 4.5: Settling time results

In figure 4.6, the steady state error was plotted after 3 seconds of the step input, the steady state error shows the difference between measured and desired input. This value is an important specification showing the ability of a system of reaching high positioning accuracy. Obviously, the smaller the steady state error is the better for our system, in our case the maximum error reported was at 0.1 m step size with a 3.81×10^{-8} m error value.

This accuracy in measuring the steady state error and the above parameters is mainly dependent on the measuring resolution of the linear encoder used. The HEIDENHAIN absolute sensor used has a measuring step resolution of 10 nm. The accuracy we reached does not express the real world accuracy and it is related to our sensor because our sensor can only guarantee for 3 μm real world accuracy.

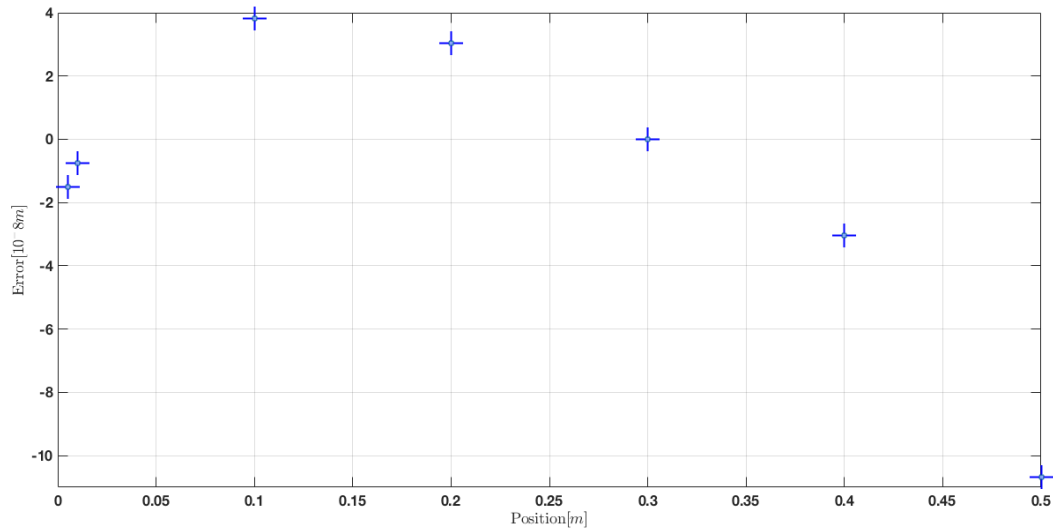


FIGURE 4.6: Steady state error.

The step response test was also performed with MES sensor we had for the linear axis system. The obtained results of the steady state error were in the order of μm , ranging between 140 and 245 μm . A notable shift in the accuracy positioning is shown with the steady state error revealing the high impact of the linear absolute encoder used with the new mechanical assembly.

4.3 Test Movements

4.3.1 Minimum Velocity

The minimum velocity our system reached with the redesigned structure and absolute sensor was 25 $\mu\text{m}/\text{s}$ as shown in figure 4.7. Moving smoothly with small step sizes requires a slow velocity and this is crucial for our application giving our robot arm the ability move smoothly along the linear axis. This value compared with the 0.01 m/s reached with the previously existing system shows an improvement in performance and robustness. Although this value is not the final value of the minimum velocity we can reach. We terminated our test at this value due to the elongated time needed to perform this type of test.

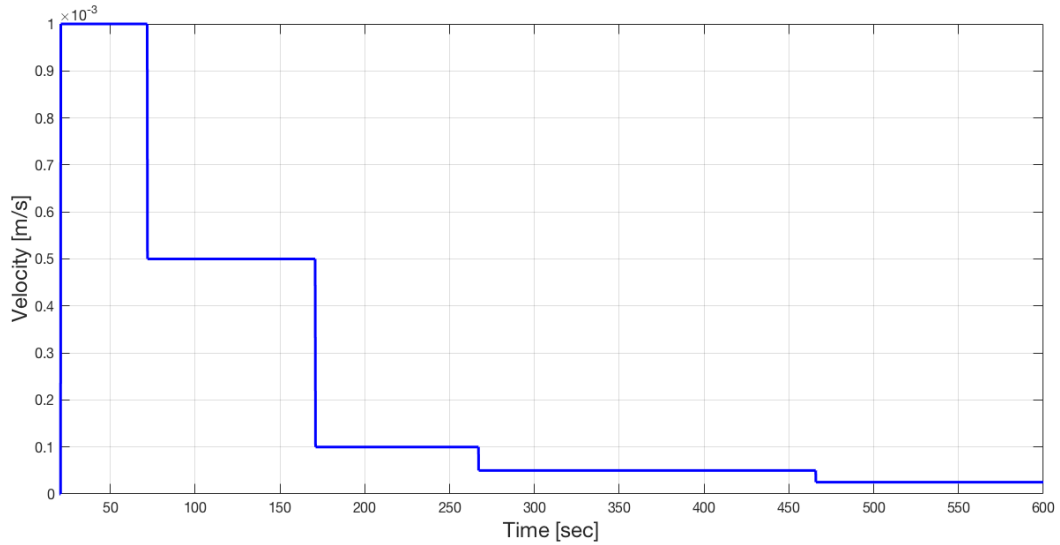


FIGURE 4.7: Minimum velocity test performed, starting with a velocity of 1 mm/s to reach a minimum of 25 μm .

4.3.2 Demonstration Trajectory

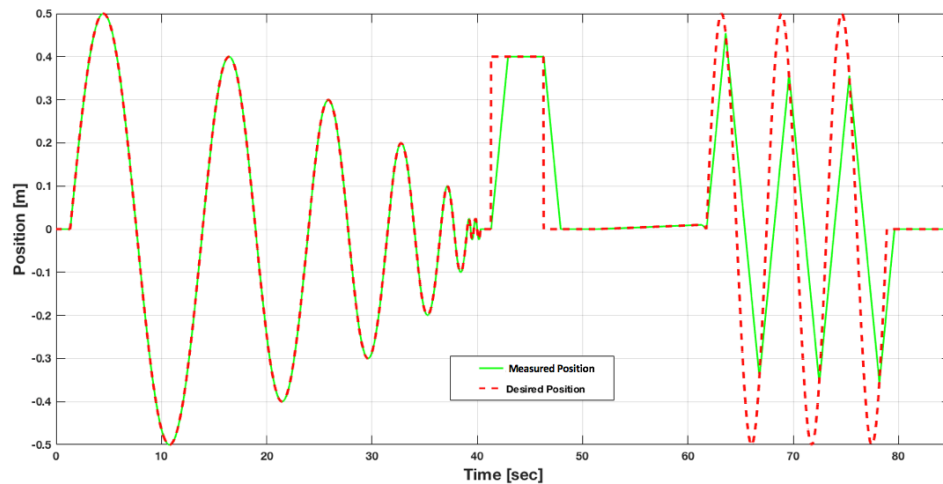


FIGURE 4.8: Figure showing both desired and measured trajectories.

In the first interval of our trajectory (0 sec to 40 sec) the actual position signal is following accurately the desired input signal with no phase shift or attenuation. This performance is highly dependent on the amplitude and frequency used for the sine wave with the velocity limit of our system. This means that the system responds perfectly to the input signal which is a main requirement of our system.

In the second interval (40 sec to 50 sec) we see that the actual signal is increasing linearly to reach the desired input step value, the same for the step down as shown. The main reason of this type of motion is due to the limit in the output velocity of 0.25 m/s we set for our linear motor. The system can not exceed this value to reach the step value

with minor rise time. The measured overshoot at step size 0.4 m as seen in section 4.2 was 3.22×10^{-4} m.

In the third interval (53 sec to 63 sec) the system moved at the selected input velocity 1×10^{-3} m/s for 10 sec and returned back to center of the axis. Even at this value of velocity, the system was moving smoothly to reach the desired position.

In last interval (63 sec to 80 sec), at $\omega = 1.1$ rad/s the attenuation increased with a shift in the output signal from input. It showed that the desired position signal failed to follow the desired sine wave at the cut-off frequency. A loss in amplitude of the sine wave was shown clearly with a phase shift between the two signals. Our system was not able to operate properly beyond the cut-off frequency and even with a close value to 1.1 rad/s. The last part of the trajectory confirmed the results we have seen in the Bode plots.

The full trajectory was a demonstration of the system characterization done in the previous chapter. The experiments shown in the above trajectory were based on the initial condition we had for the output velocity. Any change in the velocity limit will generate different results of system characterization. The maximum output velocity has a direct influence on the frequency in case of a periodic signal used. Similarly, in the step response we will obtain different results concerning rise time and other parameters in case the velocity limit of the linear motor was modified.

4.3.3 Centered Weight

With the additional weight the system was moving with an appropriate performance, but a disturbing noise started increasing slightly during the motion. This action demonstrated that the added weight created an inertia and increased friction between the ball bearing carriages and the guide rails. This phenomenon has a direct influence on the system controller, where the tuned values with no load added to the system are not performing well under the new conditions. Moving with velocity higher than 1 cm/s for an extended length will result in higher disturbing noise which is unlikely in our case.

The linear guide rails with recirculating ball bearings used in building our system have a high load-carrying capacity as given in the manufacturer manual. They can accommodate high loads and torque loads with minimum friction and handle a maximum velocity of 5 m/s. However, to attain the best of our system, the mechanical assembly and control algorithm are major factors that influence this performance. When the linear axis system is operating with a load, torque loads occurs with the acceleration and deceleration of the load and not only due to gravity. With controller tuning we can

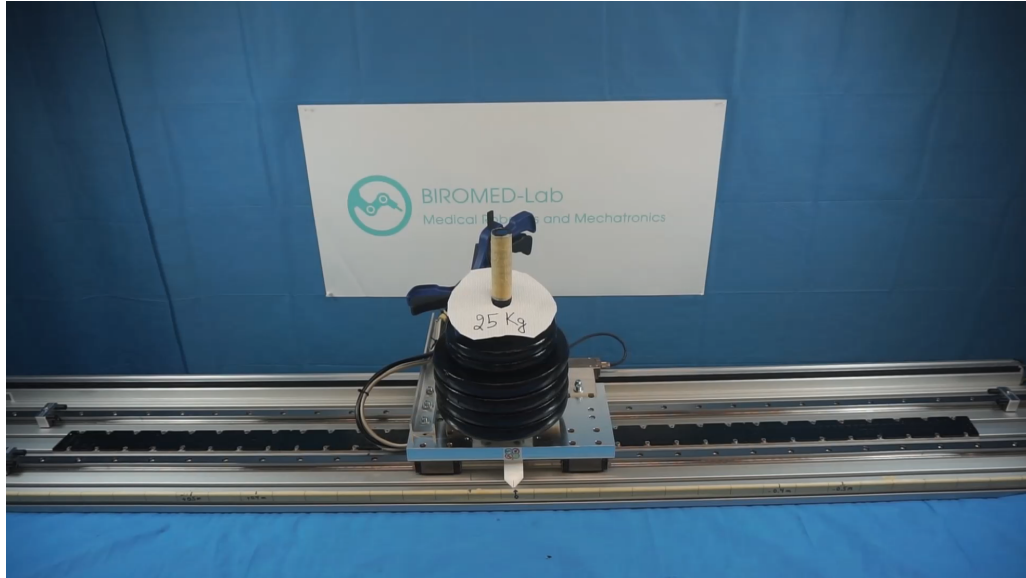


FIGURE 4.9: Centered weight of 25 Kg added to the system for testing performance.

compensate this influence. Thus, based on the observed reaction of our load condition the controller parameters have to be tuned again to result in a better performance with the new configuration.

4.4 Admittance Control

Both evaluation tests were performed in OFF and ON modes. In OFF mode high force needed to be exerted to move the carriage, due to the friction between the bearing carriages and the rail and also due to the attraction force generated between the permanent magnets and the coil even when the linear servo motor is switched off. The attraction force created between the two parts is directed downward and has an approximate value of $900N$ as given in the manufacturer manual. These factors make it hard to move the carriage in a passive way without the implementation of a force/velocity control algorithm.

In ON mode the system was responding smoothly to the applied force using the joystick. We tried to apply a higher force to the joystick resulting in a higher force measured by the sensor, but obviously the system was able to run with a maximum constant speed (25 cm/s). This is due to the limited range of applied forces in our control algorithm, no higher velocity will be generated if the force applied exceeds 5 N . Furthermore, slow and smooth movements could be done comfortably even for short distances which we were not able to do in the OFF mode of the admittance control.

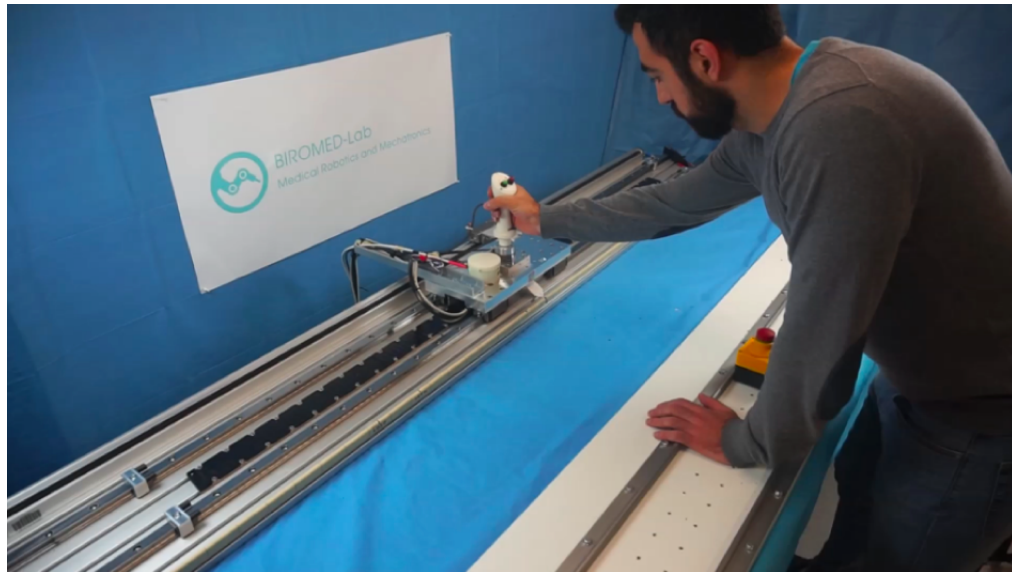


FIGURE 4.10: Admittance control evaluation test.

The test showed a satisfying reaction. However, the performance examined in the test above is dependent on the F/T sensor positioning and the way the force was applied. The test was limited with the only case of the joystick mounted to the top of the aluminium carriage. The proportional gain used in the control algorithm for the admittance control has to be tuned again in case the F/T sensor is mounted directly to robot arm.

Chapter 5

Conclusion

The thesis work results in a reliable full functioning linear axis system for the surgical robot GG-1.

Based on the conducted research on existing surgical robotic systems and robots design structures, we realized that none of these systems had combined the feature of linear axis system. From the comparison of the GG-1 robotic platform with other robots intended for medical use, we revealed the main advantages and drawbacks of the use this feature in the operating room.

In order to better understand the linear axis system we reviewed its main components and evaluated its initial state. Based on the analysis of the initial prototype we detected the main defects and defined main requirements for the new design to solve the issues with the previous system.

After the full assembly of the new system we performed a series of tests to show the accuracy in positioning and the new system performance in different conditions. Before proceeding with the tests we tuned our controller parameters which showed a satisfactory working performance despite the limitation in velocity we set to our linear motor. The results of the step response demonstrated a notable improvement in steady state error compared to the previous system considering it as a main factor in positioning accuracy relative to our linear absolute encoder.

Based on the results of the test movements we performed, the minimum velocity test revealed the capability of the new designed system. With the recorded value in minimum velocity it reached we showed that even small steps can be achieved confidently. In the demonstration trajectory performed we aimed to proof the ability of the system in following a desired trajectory. Our measured results showed a high accuracy in following

the desired trajectory and also it revealed the system limitations under the defined parameters derived from the bode plot previously with velocity restriction.

Even though the admittance control concept will be implemented later in future projects for the robot arm. The evaluation tests of admittance control we executed for our linear axis showed a good performance with a smooth motion control.

To conclude, the goals of the thesis were fulfilled successfully, the developed linear axis system is reliable in terms of mechanical structure and control algorithm regarding our configured parameters. No homing is needed anymore with the absolute encoder system installed. The developed linear axis system is ready to be integrated to the GG-1 robot arm. Nevertheless, controller tuning is recommended and required when the robot arm is mounted to the linear axis.

Although, none of the surgical robot systems developed or in research stage have used the concept of an additional linear axis to the robot system. Many challenges still need to be investigated. Miniaturization, sterilization and mounting options are some of the challenges to be considered when implementing the above concept. Mounting the current system to the ceiling would be an acceptable idea, but still enough work has to be done for example in terms of weight compensation and safe setup. This innovative idea is promising for the future and can be inspiring for other expected projects in the field. The proposed work was a starting point for the future projects in redesigning the entire robotic platform.

Appendix A

Data sheets

In this section the data sheets and properties of the implemented devices used in the thesis are listed below.



Specifications	LC 115 	LC 115	LC 185
Measuring standard Coefficient of linear expansion	DIADUR glass scale with absolute track and incremental track, grating period 20 μm $\alpha_{\text{therm}} \approx 8 \times 10^{-9} \text{ K}^{-1}$		
Accuracy grade*	$\pm 3 \mu\text{m}$ up to 3040 mm measuring length; $\pm 5 \mu\text{m}$		
Measuring length ML* in mm	140 240 340 440 540 640 740 840 940 1040 1140 1240 1340 1440 1540 1640 1740 1840 2040 2240 2440 2640 2840 3040 3240 3440 3640 3840 4040 4240		
Functional safety for applications up to	<ul style="list-style-type: none"> SIL-2 according to EN 61 508 Category 3, PL "d" according to EN ISO 13 849-1:2008 	–	
PFH	15×10^{-9} ; <i>ML > 3040 mm</i> : 25×10^{-9} (up to 6000 m above sea level)	–	
Safe position ¹⁾	<i>Encoder</i> : $\pm 550 \mu\text{m}$; <i>ML > 3040 mm</i> : $\pm 2050 \mu\text{m}$ (safety-related meas. step SM = 220 μm)	–	
	<i>Mechanical connection</i> : fault exclusions for loosening of the housing and scanning unit (page 21)		
Interface	EnDat 2.2		
Ordering designation	EnDat22		EnDat02
Measuring step <i>At $\pm 3 \mu\text{m}$</i> <i>With $\pm 5 \mu\text{m}$</i>	0.001 μm 0.010 μm		0.005 μm 0.010 μm
Clock freq. (calc. time t_{cal})	$\leq 16 \text{ MHz}$ ($\leq 5 \mu\text{s}$)		$\leq 2 \text{ MHz}$ ($\leq 5 \mu\text{s}$)
Incremental signals	–		$\sim 1 \text{ V}_{\text{PP}}$ (20 μm)
Cutoff frequency –3 dB	–		$\geq 150 \text{ kHz}$
Electrical connection	Separate adapter cable (1 m/3 m/6 m/9 m) connectable at either end of mounting block		
Cable length	$\leq 100 \text{ m}^{2)}$		$\leq 150 \text{ m}^{2)}$
Voltage supply	DC 3.6 V to 14 V		
Power consumption (max.)	3.6 V: $\leq 1.1 \text{ W}$; 14 V: $\leq 1.3 \text{ W}$		
Traversing speed	$\leq 180 \text{ m/min}$ (max. acceleration in measuring direction $\leq 100 \text{ m/s}^2$)		
Required moving force	$\leq 4 \text{ N}$		
Vibration 55 Hz to 2000 Hz affecting the Shock 11 ms	<i>Housing</i> : $\leq 200 \text{ m/s}^2$ (EN 60068-2-6) <i>Scanning unit</i> : $\leq 200 \text{ m/s}^2$ (EN 60068-2-6) $\leq 300 \text{ m/s}^2$ (EN 60068-2-27)		
Operating temperature	0 °C to 50 °C		
Protection EN 60529 ³⁾	IP 53 when installed according to instructions in the brochure, IP 64 with sealing air from DA 400		
Mass	0.55 kg + 2.9 kg/m measuring length		

* Please select when ordering

¹⁾ Further tolerances may occur in subsequent electronics after position value comparison (contact manufacturer)

²⁾ With HEIDENHAIN cable; clock frequency $\leq 8 \text{ MHz}$

³⁾ In the application the LC must be protected from the intrusion of particles and liquids

FIGURE A.1: LC 115 data sheet from HEIDENHAIN manual

6.3 Standard features

Machine concept



The AL2xxx linear servomotor series from Beckhoff is not a self-contained system. It includes various components such as a coil unit and magnetic plates and must be integrated into a complete machine concept or a complete working unit.

The size and shape of the carrier frame, the design of the carriage, the type of rail and type of bearings, and the kind of buffer used depend on the application. The carrier frame and the carriage must be designed such that an air gap is created between the coil unit and the magnetic plate.

6.3.1 Coil unit, primary part (N/S)

Winding types



The N-type (normal winding) represents the preferred type. The S-type (speed winding) has a higher maximum speed and a higher current consumption. The dimensions of the N-type and S-type do not differ.

6.3.2 Magnetic plate, secondary part

Magnetic plates are available in various lengths and can be combined with one another as desired within a series. Different series require magnetic plates with different widths.

Magnetic plate without transport plate



Magnetic plate with transport plate



In the delivery condition the magnetic plates are covered by a transport plate. It reduces the magnetic field and thus enables simple mounting and dismounting.

Specifications and dimensional drawings can be found in the chapter: [Technical data](#) [▶ 47]

BECKHOFF

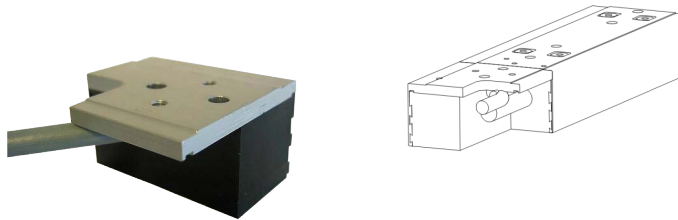
Technical description

6.3.3 Magnetic Encoder System (MES) (optional)

The Magnetic Encoder System (MES) **AL2200-000y** is a position measuring system. It has an accuracy of 0.1 mm and works directly on the magnetic plates. There are no further measuring scales. Fastening takes place on the carriage.

Description of the position measuring system

The MES works absolute within the pole distance (24 mm) and semi-absolute over the entire track. The distance to the coil part is not relevant. The commutation angle is determined once during commissioning. The wake & shake at the start of the machine is thus dispensed with. Homing can be carried out if an absolute synchronization is desired.

**Documentation for the Magnetic Encoder System (MES)!**

Further information on the Magnetic Encoder System (MES) can be found on the Beckhoff homepage under: [MES Feedback Documentation](#) or in the Beckhoff Online Information System.

6.4 Additional equipment

You require further components for the proper installation of your linear servomotor.

These are not included in the scope of delivery.

Screws and locating pins

The screws and locating pins are needed to position and fasten the coil unit to the carriage, and also the magnetic plates to the carrier frame.

Attribute	AL20xx	AL24xx	AL28xx
Screws for magnetic plates (stainless)	M5x10, DIN7984	M5x10, DIN7984	M5x16, EN ISO 4762
Screws for coil unit (steel); Length depends on the thickness of the carriage	M5, EN ISO 4762	M4, EN ISO 4762	M5, EN ISO 4762
Locating pins (stainless)	5h8		

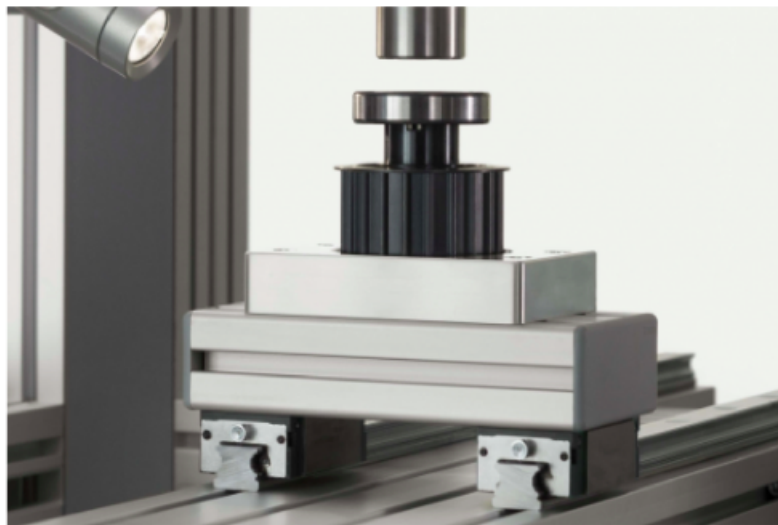
FIGURE A.2: Manual linear servomotor AL2412 from Beckhoff

Properties

The Magnetic Encoder System (MES) consists of a reader head with integrated analog Hall sensors. The Hall sensors evaluate the magnetic field of the magnetic plates and convert the signal into an analog output signal.

Name	Value / property
Signal period	Pole pair spacing 24 mm
Output signal	Analog signal 1 V _{ss} , sine-cosine
Termination resistor	R = 120 Ω
Accuracy	< 100 μm The prerequisite is the precise installation of the magnetic plates with an accuracy of ± 20 μm and offset, phase and amplitude compensation.
Repeatability	< 50 μm
Resolution	5 – 10 μm
Power supply	5 V _{DC}
Connection cable	<ul style="list-style-type: none"> • 8-core • with twisted pairs • material PUR • UL-certified • diameter 3.2 mm • length 3 m

FIGURE A.3: Magnetic Encoder System (MES) properties from Beckhoff



	PS 4-15	PS 4-20	PS 4-25
$F_y = F_z$	1000 N *	1850 N	2500 N
M_x	15 Nm	40 Nm	60 Nm
$M_y = M_z$	10 Nm	20 Nm	25 Nm
C	7200 N	13100 N	17900 N
C_D	14500 N	27000 N	37000 N
a_{max}	150 m/s ²	150 m/s ²	150 m/s ²
v_{max}	5 m/s	5 m/s	5 m/s
ϑ	-10 °C – +100 °C	-10 °C – +100 °C	-10 °C – +100 °C
h_{min}	120 mm	150 mm	180 mm

FIGURE A.4: Linear guide rails and ball bearing carriages properties from ITEM.

Bibliography

- [1] Eleanora P Westebring-van der Putten, Richard HM Goossens, Jack J Jakimowicz, and Jenny Dankelman. Haptics in minimally invasive surgery—a review. *Minimally Invasive Therapy & Allied Technologies*, 17(1):3–16, 2008.
- [2] Cost differences between open and minimally invasive surgery. URL <https://www.managedcaremag.com/archives/2015/9/cost-differences-between-open-and-minimally-invasive-surgery>. [Online, accessed: January 13, 2019].
- [3] Exploring surgery options: open vs. minimally invasive. URL <https://www.beaumont.org/health-wellness/blogs/exploring-surgery-options-open-vs-minimally-invasive>. [Online, accessed 19.08.2018].
- [4] Should we fall out of love with robot surgery?, . URL <https://www.smithsonianmag.com/innovation/should-we-fall-out-of-love-with-robot-surgery-22444515/>. [Online, accessed: January 16, 2019].
- [5] John A Repicci and RW Eberle. Minimally invasive surgical technique for unicompartmental knee arthroplasty. *Journal of the Southern Orthopaedic Association*, 8(1): 20–7, 1999.
- [6] Robotic endoscope for laser osteotomy/end-effector stabilization in minimally invasive surgery, . URL <https://dbe.unibas.ch/en/research/laser-and-robotics/bio-inspired-robots-for-medicine-lab/robotic-endoscope-for-laser-osteotomyend-effector-stabilization-in-minimally-invasive-surgery/>. [Online, accessed: January 16, 2019].
- [7] Jess H Lonner, Thomas K John, and Michael A Conditt. Robotic arm-assisted uka improves tibial component alignment: a pilot study. *Clinical Orthopaedics and Related Research®*, 468(1):141, 2010.
- [8] . URL <https://www.stryker.com/us/en/portfolios/orthopaedics/joint-replacement/mako-robotic-arm-assisted-surgery.html>. [Online, accessed: January 16, 2019].

- [9] Computer-assisted total knee and robotic-assisted partial knee surgery: Sharing the benefits of these techniques with medical professionals from other countries, . URL <https://holycrossleonecenter.com/blog/computer-assisted-total-knee-and-robotic-assisted-partial-knee-surgery-sharing-the-benefits-of-these-techniques-with-medical-professionals-from-other-countries/>. [Online, accessed: January 16, 2019].
- [10] Laser-cutting of bones replaces sawing. URL <https://www.news.admin.ch/news/message/attachments/40898.pdf>. [Online, accessed: October 31, 2018].
- [11] Alfredo E Bruno, Hans-Florian Zeilhofer, and Philipp Jürgens. Carlo-computer assisted and robot guided laser-osteotome, August 30 2012. US Patent App. 13/497,520.
- [12] . URL <https://aot.swiss/en/carlo/>. [Online, accessed: January 17, 2019].
- [13] Marco Ceccarelli and Erika Ottaviano. Design problems for parallel manipulators in assembling operations. *IFAC Proceedings Volumes*, 36(23):13–26, 2003.
- [14] Jean-Pierre Merlet. *Parallel robots*, volume 128. Springer Science & Business Media, 2006.
- [15] Roboy 2.0 - inverse kinematics, . URL <https://roboy-ik-doc.readthedocs.io/en/latest/>. [Online, accessed: January 16, 2019].
- [16] Inverse kinematics solution of a robotic arm using ml, . URL <https://cvexplorare.wordpress.com/2016/11/14/inverse-kinematics/#more-19>. [Online, accessed: January 16, 2019].
- [17] Richard Hartenberg and Jacques Danavit. *Kinematic synthesis of linkages*. New York: McGraw-Hill, 1964.
- [18] Lung-Wen Tsai. *Robot analysis: the mechanics of serial and parallel manipulators*. John Wiley & Sons, 1999.
- [19] IA Bonev and Dimiter Zlatanov. The mystery of the singular snu translational parallel robot. *ParalleMIC Reviews*, (4), 2001.
- [20] Alain Codourey, Marcel Honegger, and Etienne Burdet. A body-oriented method for dynamic modeling and adaptive control of fully parallel robots. In *Proceedings of 5th Symposium on Robot Control*, pages 443–450. Citeseer, 1997.
- [21] JM Selig and P Ross McAree. Constrained robot dynamics ii: Parallel machines. *Journal of robotic systems*, 16(9):487–498, 1999.

- [22] W Khalil and S Guegan. A new method for the dynamic formulation of parallel manipulators. *Journées Franco-Mexicaines d'automatique appliquée, 12-14 Septembre*, 2001.
- [23] Robotica paralela delta, . URL <http://www.robotic-lab.com/blog/2006/11/26/robotica-paralela-delta/>. [Online, accessed: January 16, 2019].
- [24] Nicolae Plitea, Dorin Lese, Doina Pisla, and Calin Vaida. Structural design and kinematics of a new parallel reconfigurable robot. *Robotics and computer-integrated manufacturing*, 29(1):219–235, 2013.
- [25] Sébastien Briot and Ilian A Bonev. Are parallel robots more accurate than serial robots? *Transactions of the Canadian Society for Mechanical Engineering*, 31(4):445–455, 2007.
- [26] Ilian Bonev. Delta parallel robot the story of success. *Newsletter, available at <http://www.parallelmic.org>*, 2001.
- [27] Tanio K Tanev. Kinematics of a hybrid (parallel–serial) robot manipulator. *Mechanism and Machine Theory*, 35(9):1183–1196, 2000.
- [28] Azamat Yeshmukhametov, Maksat Kalimoldayev, Orken Mamyrbayev, and Yedilhan Amirgaliev. Design and kinematics of serial/parallel hybrid robot. In *Control, Automation and Robotics (ICCAR), 2017 3rd International Conference on*, pages 162–165. IEEE, 2017.
- [29] Azamat Yeshmukhametov, Maksat N. Kalimoldayev, Orken J. Mamyrbayev, and Yedilhan Amirgaliev. Design and kinematics of serial/parallel hybrid robot. *2017 3rd International Conference on Control, Automation and Robotics (ICCAR)*, pages 162–165, 2017.
- [30] Allen L Feng, Christopher R Razavi, Pranav Lakshminarayanan, Zaid Ashai, Kevin Olds, Marcin Balicki, Zhen Gooi, Andrew T Day, Russell H Taylor, and Jeremy D Richmon. The robotic ent microsurgery system: A novel robotic platform for microvascular surgery. *The Laryngoscope*, 127(11):2495–2500, 2017.
- [31] Yik San Kwok, Joahin Hou, Edmond A Jonckheere, and Samad Hayati. A robot with improved absolute positioning accuracy for ct guided stereotactic brain surgery. *IEEE Transactions on Biomedical Engineering*, 35(2):153–160, 1988.
- [32] Kevin Cleary and Charles Nguyen. State of the art in surgical robotics: clinical applications and technology challenges. *Computer Aided Surgery*, 6(6):312–328, 2001.

- [33] R. A. Faust D. J. Terris N. G. Hockstein, C. G. Gourin. A history of robots: from science fiction to surgical robotics. *Journal of Robotic Surgery*, 1:113–118, 2007.
- [34] A brief history, . URL <https://allaboutroboticsurgery.com/surgical-robots.html>. [Online, accessed: January 16, 2019].
- [35] Surgical robots operate with precision. URL <https://www.wired.com/2009/09/surgical-robots/>. [Online, accessed: October 17, 2018].
- [36] Eric J. Moore. Robotic surgery. URL <https://www.britannica.com/science/robotic-surgery>. [Online, accessed: October 17, 2018].
- [37] SJ Harris, F Arambula-Cosio, Q Mei, RD Hibberd, BL Davies, JEA Wickham, MS Nathan, and B Kundu. The probotan active robot for prostate resection. *Proceedings of the Institution of Mechanical Engineers, Part H: Journal of Engineering in Medicine*, 211(4):317–325, 1997.
- [38] J Cobb, J Henckel, P Gomes, S Harris, M Jakopec, F Rodriguez, A Barrett, and B Davies. Hands-on robotic unicompartmental knee replacement: a prospective, randomised controlled study of the acrobot system. *The Journal of bone and joint surgery. British volume*, 88(2):188–197, 2006.
- [39] The future of surgical precision, . URL <https://toc.com.sg/the-future-of-surgical-precision/>. [Online, accessed: January 16, 2019].
- [40] Jger C. Kraft K. et al. Kraft, B.M. The aesop robot system in laparoscopic surgery: Increased risk or advantage for surgeon and patient? *Journal of Robotic Surgery*, 2004. URL <https://doi.org/10.1007/s00464-003-9200-z>.
- [41] Robotic surgery, . URL <https://spinoff.nasa.gov/spinoff2000/hm1.htm>. [Online, accessed: January 17, 2019].
- [42] Garth H Ballantyne and Fred Moll. The da vinci telerobotic surgical system: the virtual operative field and telepresence surgery. *Surgical Clinics*, 83(6):1293–1304, 2003.
- [43] Cinzia Freschi, Vincenzo Ferrari, Franca Melfi, Mauro Ferrari, F Mosca, and A Cuschieri. Technical review of the da vinci surgical telemanipulator. *The International Journal of Medical Robotics and Computer Assisted Surgery*, 9(4):396–406, 2013.
- [44] Da vinci surgical robot, . URL <https://robocatz.com/daVinci-surgical.htm>. [Online, accessed: January 17, 2019].

- [45] Gyung Tak Sung and Inderbir S Gill. Robotic laparoscopic surgery: a comparison of the da vinci and zeus systems. *Urology*, 58(6):893–898, 2001.
- [46] Comparison of s si robots, breakthrough platforms from da vinci surgical systems, . URL <https://laser-prostate-robot.co.uk/prostate-cancer/robotised-prostatectomy/comparison-of-s-si-robots-versions/>. [Online, accessed: January 17, 2019].
- [47] James Chi-Yong Ngu, Charles Bih-Shiou Tsang, and Dean Chi-Siong Koh. The da vinci xi: a review of its capabilities, versatility, and potential role in robotic colorectal surgery. *Robotic Surgery: Research and Reviews*, 4:77–85, 2017.
- [48] Woo-Jung Lee, Severance Robot, and MIS Center. Ten-year experience of the da vinci robotic surgery at severance yonsei university hospital in korea. *Hanyang Medical Reviews*, 36(4):215–224, 2016.
- [49] URL <https://www.intuitive.com/en/products-and-services/da-vinci>. [Online, accessed: October 18, 2018].
- [50] Intuitive surgical announces innovative single port platform the da vinci sp surgical system. URL https://scholar.google.it/scholar?hl=en&as_sdt=0%2C5&q=Intuitive+Surgical+Announces+Innovative+Single+Port+Platform+%E2%80%94+the+da+Vinci+SP%C2%AE+Surgical+System&btnG=. [Online, accessed: December 17, 2018].
- [51] . URL <https://www.intuitive.com/en/products-and-services/da-vinci/systems/sp>. [Online, accessed: January 17, 2019].
- [52] Computer motion to start patent infringement war on medical robotics against intuitive surgical. URL <http://www.hoise.com/vmw/00/articles/vmw/LV-VM-07-00-18.html>. [Online, accessed: October 30, 2018].
- [53] Patrick Aidan and Maroun Bechara. Gasless trans-axillary robotic thyroidectomy: the introduction and principle. *Gland surgery*, 6(3):229, 2017.
- [54] . URL <https://www.stryker.com/us/en/portfolios/orthopaedics/joint-replacement/mako-robotic-arm-assisted-surgery.html>. Online, accessed: December 17, 2018].
- [55] The galen surgical system, . URL <http://surgrob.blogspot.com/2017/02/the-galen-surgical-system.html>. [Online, accessed: December 17, 2018].
- [56] Galen mk1 hamlyn 090418 lowrez, . URL <https://www.youtube.com/watch?v=hZP5QHx19dc>. [Online, accessed: January 17, 2019].

- [57] Telem manipulation in minimally invasive surgery, . URL https://www.dlr.de/rm/en/desktopdefault.aspx/tabid-3795/16616_read-40529/. [Online, accessed: December 17, 2018].
- [58] Miro, . URL <https://www.dlr.de/rm/en/desktopdefault.aspx/tabid-11673/#gallery/29806>. [Online, accessed: January 17, 2019].
- [59] Cmr reveals their versius robot, . URL <http://surgrob.blogspot.com/2016/12/cmr-reveals-their-versius-robot.html>. [Online, accessed: December 17, 2018].
- [60] Meet versius, cambridge medical robotics portable and cost effective robot for minimal access surgery, . URL <https://www.medgadget.com/2017/11/cambridge-medical-robotics-minimal-access-surgery-versius.html>. [Online, accessed: January 17, 2019].
- [61] Nicola Preda, Auralius Manurung, Olivier Lamercy, Roger Gassert, and Marcello Bonfè. Motion planning for a multi-arm surgical robot using both sampling-based algorithms and motion primitives. In *Intelligent Robots and Systems (IROS), 2015 IEEE/RSJ International Conference on*, pages 1422–1427. IEEE, 2015.
- [62] Robotic platform for autonomous surgery, . URL <http://www.relab.ethz.ch/research/past-research-projects/robotic-platform-for-autonomous-surgery.html>. [Online, accessed: January 17, 2019].
- [63] Transforming robotic components into innovative medical solutions, . URL <https://www.nature.com/articles/d42473-018-00004-4>. [Online, accessed: January 17, 2019].
- [64] . URL <https://www.universal-robots.com/products/ur3-robot/>. [Online, accessed: January 17, 2019].
- [65] Telem manipulation in minimally invasive surgery, . URL https://www.dlr.de/rm/en/desktopdefault.aspx/tabid-3795/16616_read-40529/. [Online, accessed: January 17, 2019].
- [66] . URL <https://www.kuka.com/en-de/products/robot-systems/robot-periphery/linear-units>. [Online, accessed: January 17, 2019].
- [67] Yi Cao, Ke Lu, Xiujuan Li, and Yi Zang. Accurate numerical methods for computing 2d and 3d robot workspace. *International Journal of Advanced Robotic Systems*, 8(6):76, 2011.
- [68] U Horas, D Pelinkovic, G Herr, T Aigner, and R Schnettler. Autologous chondrocyte implantation and osteochondral cylinder transplantation in cartilage repair of the knee joint: a prospective, comparative trial. *JBJS*, 85(2):185–192, 2003.

- [69] Usns mercy surgical team, sri lankan surgical team perform first robot-assisted surgery aboard a ship. URL <https://www.dvidshub.net/image/4362763/usns-mercy-surgical-team-sri-lankan-surgical-team-perform-first-robot-assisted-surgery-aboard-ship>. [Online, accessed: January 18, 2019].
- [70] Strengths limitations: Belt drive vs. ball screw actuators, . URL <http://blog.misumiusa.com/strengths-limitations-belt-drive-vs-ball-screw-actuators/>. [Online, accessed: January 18, 2019].
- [71] Rack and pinion drive system: What is it? URL <https://www.motioncontroltips.com/what-is-a-rack-and-pinion/>. [Online, accessed: January 18, 2019].
- [72] High performance, simple linear units with steel re-enforced driving belt, . URL <https://www.rollon.com/IN/en/products/actuator-line/11-smart-system/>. [Online, accessed: January 18, 2019].
- [73] Linear and rotary compared. URL https://infosys.beckhoff.com/english.php?content=../content/1033/al_grundlagen/2036411275.html&id=. [Online, accessed: January 18, 2019].
- [74] How does a linear motor work? URL https://www.youtube.com/watch?v=0_QB16-_jJU. [Online, accessed: January 18, 2019].
- [75] Paul Sandin. *Robot mechanisms and mechanical devices illustrated*. McGraw Hill Professional, 2003.
- [76] Why lead screws are the best fit for many linear motion applications - and how to rightly apply them. URL https://www.thomsonlinear.com/downloads/articles/Why_Lead_Screws_Best_Fit_Linear_Motion_Applications.taen.pdf. [Online, accessed: November 14, 2018].
- [77] The ball screw vs. lead screw, . URL <http://multicam.ca/the-ball-screw-vs-lead-screw/>. [Online, accessed: January 18, 2019].
- [78] Linear actuators:belt driven vs. rack and pinion driven. URL <https://www.linearmotiontips.com/linear-actuators-belt-driven-vs-rack-and-pinion-driven/>. [Online, accessed: November 14, 2018].
- [79] . URL <http://doormartgaragedoors.com/2013/09/13/chain-drive-v-s-screw-drive-v-s-belt-drive/>. [Online, accessed: January 18, 2019].
- [80] Seamus Gordon and Michael T Hillery. Development of a high-speed cnc cutting machine using linear motors. *Journal of Materials Processing Technology*, 166(3): 321–329, 2005.

- [81] Parker Hannifin Jim Monnich. The nuts bolts of selecting the correct linear drive train. URL <https://www.ecnmag.com/article/2014/05/nuts-bolts-selecting-correct-linear-drive-train>. [Online, accessed: January 18, 2019].
- [82] URL <https://txpbearing.en.made-in-china.com/product/mjBQGfaobEhd/China-Hot-Sale-and-High-Precision-Aluminum-Round-Linear-Rail-for-CNC-Machine.html>. [Online, accessed: January 18, 2019].
- [83] Round or square? URL <https://www.machinedesign.com/archive/round-or-square>. [Online, accessed: November 19, 2018].
- [84] Thomson linear motion. URL <http://www.directindustry.com/prod/thomson-industries-inc/product-7040-55560.html>. [Online, accessed: January 18, 2019].
- [85] When to go linear. URL <https://www.machinedesign.com/archive/when-go-linear>. [Online, accessed: December 18, 2018].
- [86] Encoders open the way for new applications, . URL <http://industrial.embedded-computing.com/article-id/?4408>. [Online, accessed: January 18, 2019].
- [87] Neville Hogan. Impedance control: An approach to manipulation. In *American Control Conference, 1984*, pages 304–313. IEEE, 1984.
- [88] Linear encoders for numerically controlled machine tools. URL https://www.heidenhain.de/fileadmin/pdb/media/img/571470-2B_Linear_Encoders_For_Numerically_Controlled_Machine_Tools.pdf. [Online, accessed: January 18, 2019].
- [89] Optional encoder card, . URL https://infosys.beckhoff.com/english.php?content=../content/1033/ax5000_system_doku_hw2/9007202653060235.html&id=3243970956042340426. [Online, accessed: January 18, 2019].
- [90] Pid theory explained. URL <http://www.ni.com/white-paper/3782/en/>. [Online, accessed: December 6, 2018].
- [91] M Araki. Pid control. *Control Systems, Robotics and Automation: System Analysis and Control: Classical Approaches II, Unbehauen, H.(Ed.). EOLSS Publishers Co. Ltd., Oxford, UK., ISBN-13: 9781848265912*, pages 58–79, 2009.
- [92] Lino Guzzella. *Analysis and synthesis of Single-input Single-output control systems*. vdf Hochschulverlag AG, 2011.

- [93] Shankar P Bhattacharyya, Lee H Keel, and Aniruddha Datta. *Linear control theory: structure, robustness, and optimization*. CRC press, 2009.
- [94] Farid Golnaraghi and BC Kuo. Automatic control systems. *Complex Variables*, 2: 1–1, 2010.